Master Thesis

One-dimensional Study of Alfvén Waves in the Solar Chromosphere: Effects of Reflection and Magnetic Diffusion

Shunya Kono

Department of Earth and Planetary Science

Graduate School of Science, The University of Tokyo

March 1, 2015

Abstract

The solar chromosphere consists of plasma gas which has higher temperature (10^4 K) than the solar photosphere surface (6000 K) and the heating mechanism has not been understood enough. It has been suggested that Alfvén waves, generated in the photosphere and propagating along the magnetic flux tube, can carry enough energy to the low-plasma-beta region in the upper chromosphere and the dissipation of waves is one of the possible heating mechanisms. The chromosphere is partially ionized. The ambipolar diffusion is caused by the collisions between plasmas and neutrals, and considered to enhance the effect of magnetic diffusion. On the other hand, the compressible waves are generated by the nonlinear effect of the magnetic pressure associated with the Alfvén waves propagating upwards from the photosphere, and form shock waves in the chromosphere. In previous studies, it has been indicated that the dissipation of generated shock waves can give enough thermal energy to heat the chromosphere. The effect of the magnetic diffusion to the nonlinear propagation of Alfvén waves in the chromosphere has not been investigated enough. Some observations show the reflection of Alfvén waves at the transition region, which is existing at the boundary between the chromosphere and corona. It is important to discuss the dissipation mechanisms of waves in consideration of the reflection mechanism at the top and bottom boundaries of the chromosphere.

In this study, we investigate the effect of magnetic diffusion to the Alfvén waves propagating along a vertically open magnetic flux tube in the chromosphere. First, we calculate the damping length of waves which have frequencies of 10^{-3}–10^{-1} Hz by the magnetic diffusion in the solar quiet region. The length is estimated as much larger than

the thickness of the chromosphere. For the chromospheric heating, we should consider the condition where the reflection at the photosphere and transition region efficiently occurs and more Alfvén waves are trapped in the chromosphere. Next, we investigate the propagations of the nonlinear Alfvén waves by performing one-dimensional numerical simulations. As a result, 60–70 % of the incident Alfvénic pulse waves with frequencies of 0.01–0.10 Hz are reflected at the transition region. Most of reflected waves from the transition region penetrate into the convection zone without being reflected at the bottom of the photosphere. We perform simulations in different magnetic field structures and confirm that the results are almost the same in any cases. If the initial velocity amplitude of Alfvén wave is set to be 1.0 km s^{-1}, the compressible waves generated by the nonlinear effect may have enough energy to heat the chromosphere. It is considered to be important to take the energy flux going from the top and bottom boundaries of the chromosphere into account for the dissipation of Alfvén waves in the chromosphere.

要旨

太陽彩層は 10000 K と太陽光球表面（6000 K）より高温のプラズマで構成されておりその加熱機構は未だに理解されていない。特に太陽彩層上部の低プラズマベータ領域の加熱機構として、光球表面から励起される、磁束管に沿ったアルフベン波によるエネルギーの輸送と散逸の説が提唱されている。また彩層ではプラズマは部分電離状態であると考えられている。彩層中に存在する中性粒子とプラズマ粒子との衝突によって生じる両極性拡散効果は磁気拡散を強め、アルフベン波の減衰による加熱を生じさせると考えられている。一方、光球から上方へ伝播するアルフベン波に伴う磁気圧の非線形効果により生じる圧縮波は彩層中で衝撃波を形成し、その散逸により彩層加熱に十分寄与する熱エネルギーが生じることが過去の研究により示唆されている。磁気拡散がどの程度、彩層を伝播するアルフベン波の非線形過程に影響を与えるかはこれまでに十分に調べられていない。また観測により太陽彩層とコロナの境界に位置する遷移層におけるアルフベン波の反射が示唆されており、彩層上部および下部の境界における波の反射の機構を踏まえた上でその散逸過程について議論することが重要であると考えられる。

本研究では彩層中の磁束管伝播アルフベン波に対する磁気拡散の効果を調べた。まず始めに、太陽静穏領域大気構造を仮定した場合における 10^{-3}–10^{-1} Hz の周波数の波の磁気拡散による減衰距離を計算すると、その長さは彩層の厚みよりも大きいことが見積もられた。したがって磁気拡散が加熱により大きく寄与するためには、遷移層および光球表面における波の反射がより効果的に生じ、彩層中にアルフベン波がより保持されるような構造が必要となる。次に、非線形アルフベン波の伝播を 1 次元数値シミュレーションを用いて調べた。計算の結果、0.01–0.10 Hz の周波数

のアルフベン波パルスの 60–70 %が遷移層において反射されることが明らかとなった。さらに遷移層からの反射波の大部分は光球表面では反射されず、対流層へと透過していく。異なる磁場構造を設定した場合にもこの結果はほとんど変わらないことが示された。初期速度振幅が 1.0 km s^{-1} のアルフベン波を設定した場合、非線形効果により生じる圧縮波は彩層加熱に十分寄与するエネルギーを持つことが明らかとなった。彩層中におけるアルフベン波の散逸過程を考察する上では、彩層上部および下部から流出するエネルギー流束を考慮することが重要であると考えられる。

Contents

Chapter 1

Introduction

1.1 The Solar Atmosphere

The solar atmosphere consists of four characteristic layers with different properties. Figure 1.1 shows the averaged temperature distribution along the height in the solar quiet region, which is called VAL-C model (Vernazza et al., 1981). This distribution is derived from the EUV continuum and other multi-wavelength observations. The atmosphere is assumed as plane-parallel and in hydrostatic equilibrium. The zero point of height is defined as the position that optical thickness from an observer in the wavelength 500 nm becomes unity. Temperature is falling from about 6600 K at the zero point to a minimum value, which is about 4200 K, at the height of about 500 km. From zero point of height to this height of minimum temperature, the layer is defined as the *photosphere*. From the top of the photosphere, temperature rises slowly through the upper atmosphere and then dramatically above the height of about 2300 km to a few million K in the *corona* (,which the coronal temperature has been indicated in Athay, 1976). The narrow layer where temperature rises drastically to the coronal temperature is called the *transition region* and the intermediate region between the top of the photosphere and the bottom of the transition region is defined as the *chromosphere*. The layer existing below the photosphere is called the *convection zone*. In this region, the density is large and the temperature increases from

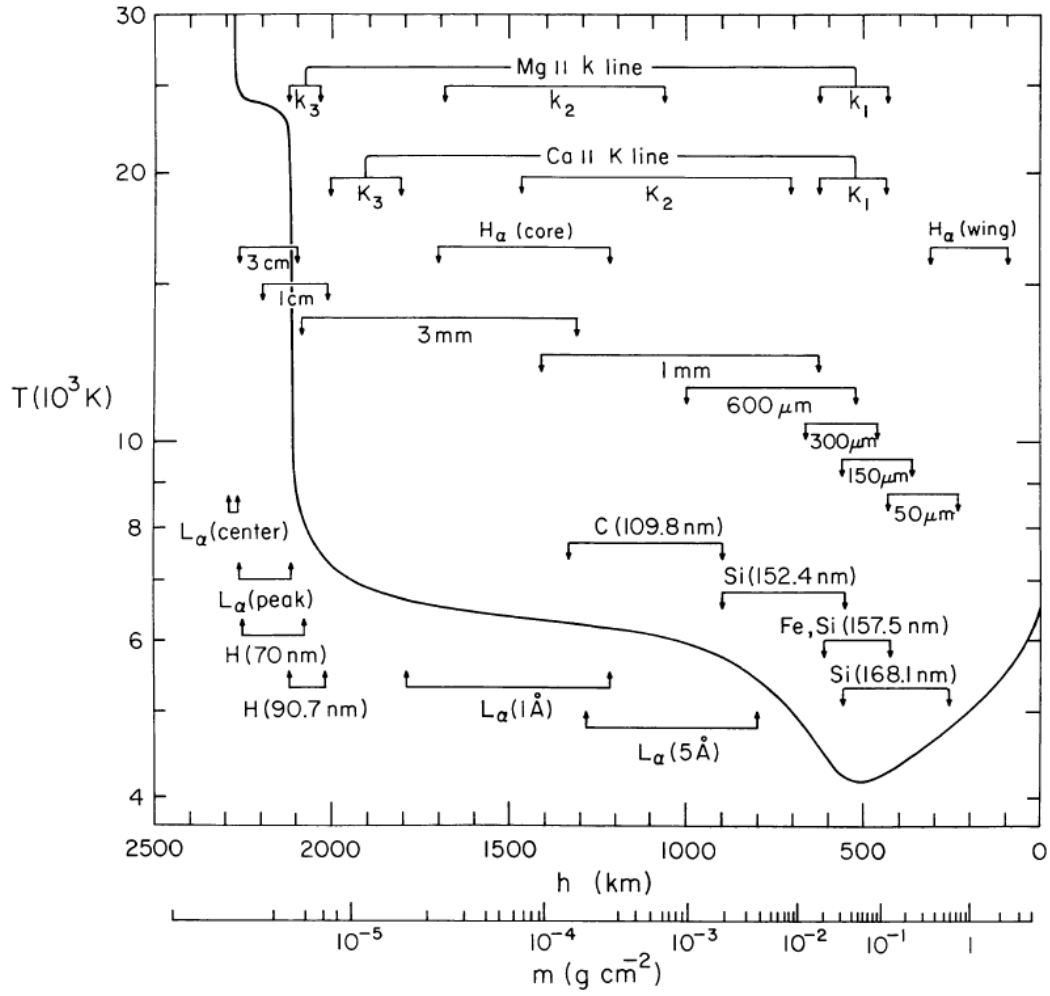

Figure 1.1: The temperature distribution in the solar quiet region. This standard solar atmospheric model is called VAL-C. The profile is derived from observations of the EUV continuum, the Lα line, and other various lines. The approximate depths where the various continua and lines originate are showed (Vernazza et al., 1981).

the zero point of height toward the center of the Sun. The layer is filled with turbulent fluid motions due to the convection.

The reason for the temperature rise above the top of the photosphere has been still unclear and one of the major problems in solar physics. This is called as " *the chromospheric and coronal heating problem* ".

1.2 Energy Losses from the Solar Atmosphere

As mentioned in Section 1.1, heating mechanism of the upper solar atmosphere (which consists of the chromosphere and corona) has been not yet understood.

Withbroe & Noyes (1977) estimated required energy to heat the chromosphere and corona. Table 1.1 compares various energy loss mechanisms for the chromosphere, transition region, and corona in three different areas (which are quiet region, coronal hole, and active region) obtained from models which are based on various observations. In order

Table 1.1: Chromospheric and coronal energy losses (Withbroe & Noyes, 1977)

Parameter	Quiet region	Coronal hole	Active region
Transition layer pressure (dyn cm^{-2})	2×10^{-1}	7×10^{-2}	2
Coronal temperature (K, at $r \approx 1.1 R_{\odot}$)	1.1 to 1.6 $\times 10^{6}$	10^{6}	2.5×10^{6}
Coronal energy losses (erg cm^{-2} s^{-1})			
Conduction flux	2×10^{5}	6×10^{4}	10^{5} to 10^{7}
Radiative flux	10^{5}	10^{4}	5×10^{6}
Solar wind flux	$\leq 5 \times 10^{4}$	7×10^{5}	$(< 10^{5})$
Total coronal loss	3×10^{5}	8×10^{5}	10^{7}
Chromospheric radiative losses (erg cm^{-2} s^{-1})			
Low chromosphere	2×10^{6}	2×10^{6}	$\geq 10^{7}$
Middle chromosphere	2×10^{6}	2×10^{6}	10^{7}
Upper chromosphere	3×10^{5}	3×10^{5}	2×10^{6}
Total chromospheric loss	4×10^{6}	4×10^{6}	2×10^{7}
Solar wind mass loss (g cm^{-2} s^{-1})	$\leq 2 \times 10^{-11}$	2×10^{-10}	$(< 4 \times 10^{-11})$

to maintain the solar atmospheric temperature profile, energy input balanced with these losses is needed. In the chromosphere, energy losses are thought to be mainly caused by

radiative cooling. Since we are interested in the mechanisms in which the temperature distribution in VAL-C model (shown in Figure 1.1) is formed, we focus on the energy losses in the solar quiet region. In the low chromosphere, which is defined as the region just above from the height of the temperature minimum at about 500 km to the height of 1000 km where the temperature is about 6000 K, the radiative losses are taken from the estimate in Athay (1976) which is 2×10^6 erg cm^{-2} s^{-1}. For the middle chromosphere, which extends upward from the top of low chromosphere to the height of 2100 km where the temperature reaches about 10^4 K, the radiative losses are also about 2×10^6 erg cm^{-2} s^{-1} (Athay, 1976) based on the measured intensities of spectral lines and continua formed there. In the upper chromosphere, which is the region between the height of 2100 km where the temperature is about 10^4 K and that of 2300 km where the temperature is about 3×10^4 K, a loss rate of about 3×10^5 erg cm^{-2} s^{-1} is yielded by hydrogen Lyman alpha emission (Athay, 1976). The total energy losses in the chromosphere is about 4×10^6 erg cm^{-2} s^{-1}, which is approximately one order of magnitude larger than that in the corona which is about 3×10^5 erg cm^{-2} s^{-1}. The chromosphere is a relatively dense region compared to the corona, which causes stronger radiative cooling, so this indicates more heating is required to maintain the chromospheric temperature.

1.3 Heating Mechanisms

1.3.1 Acoustic Wave Heating

Biermann (1948) and Schwarzschild (1948) first proposed that compressible *acoustic waves* generated by turbulent motion at the surface of the solar convection zone are one of the possible mechanisms to heat the upper solar atmosphere. Generated acoustic waves steepen to form *shock waves* as they propagate upwards and then dissipation of shock waves might contribute to heat the chromosphere and corona.

Energy flux of acoustic waves produced by turbulent convective motion was investi-

gated in Lighthill (1952, 1954). According to the theory, the power emission for homogeneous, isotropic turbulence becomes

$$P = \alpha \epsilon M^5, \tag{1.1}$$

where P is the acoustic radiative energy per unit mass and unit time, α the constant value depending on each turbulence model, ϵ the turbulence energy dissipation rate per unit mass (where the turbulence decay time scale is given as $\tau \sim v^2/\epsilon \sim l/v$, v is the turbulence velocity scale and l the turbulence length scale), and $M = v/c_S$ the Mach number (where c_S is the acoustic speed). Proudman (1952) calculated quantitatively the power for homogeneous, isotropic, decaying turbulence, obtaining $\alpha = 10$–40. Lighthill's theory was extended for stratified atmospheres in Unno & Kato (1962) or Stein (1968). Stein (1968) calculated the upward acoustic energy flux from the solar convection zone is 2×10^7 erg cm^{-2} s^{-1}, which is to be compared with estimated values for radiative losses from the chromosphere (Withbroe & Noyes, 1977).

Acoustic wave energy flux in the photosphere and chromosphere was calculated from observations of atmospheric vertical oscillations in Mein & Schmieder (1981). They used observations of Doppler-shifts at different heights where the lines of Ca II and Mg I are formed. The observations are made at the vacuum Telescope of Sacramento Peak Observatory (described in Mein & Mein, 1976; Schmieder, 1976) and focused on the quiet regions on the solar disk. They analyzed the observational data at the locations in the magnetic cells of the chromospheric network. Magnetic cells correspond to the intermediate regions between the magnetic flux tubes, so called the solar internetwork regions. The energy flux is derived from the related velocity amplitudes and phase shifts measured at each height and based on some atmospheric models in the solar quiet region. Figure 1.2 shows the acoustic wave energy flux versus the altitude from the photosphere. The flux integrated over different wave period ranges is shown. For the case of wave period 120–400 s, the acoustic wave energy flux decreases from 8×10^7 erg cm^{-2} s^{-1} in the

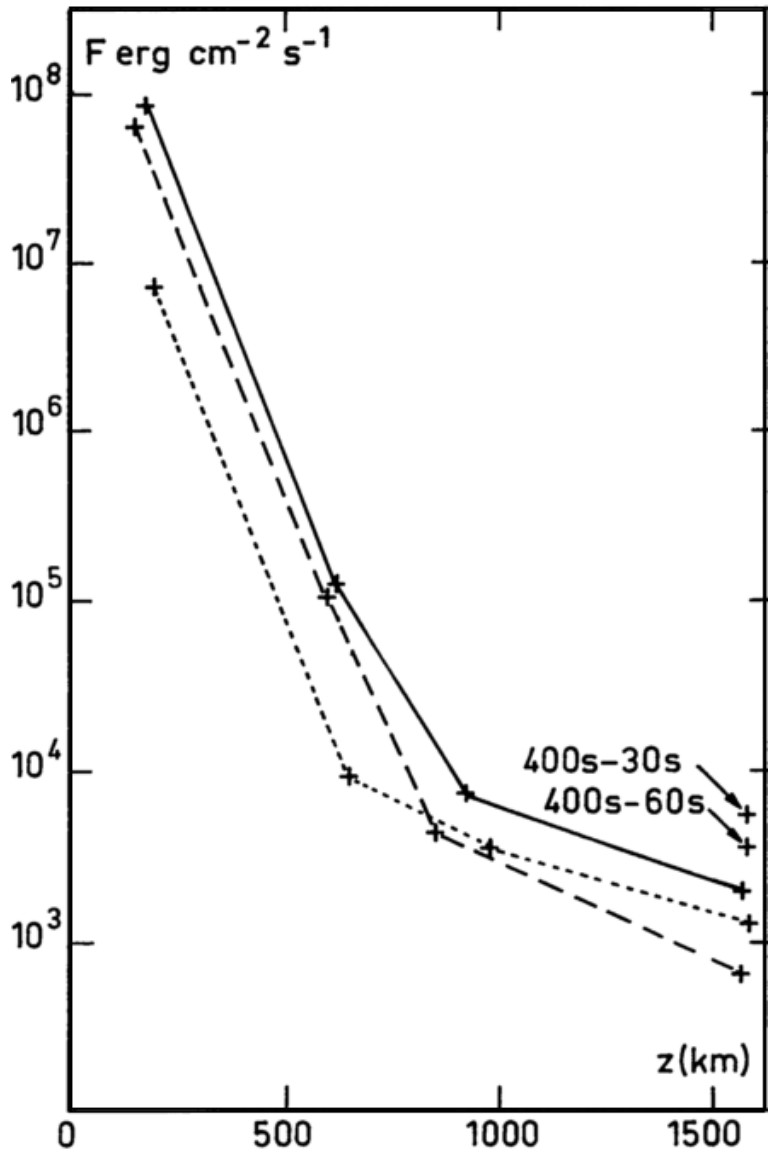

Figure 1.2: Variation of acoustic wave energy flux along vertical direction from the photosphere to the middle chromosphere calculated from observations of Doppler-shifts in Ca_{II} and Mg_{I} lines. Each line shows in different wave period ranges: solid line 120–400 s, dashed line 200–400 s, dotted line 120–200 s (for 1500 km, two more ranges are compared) (Mein & Schmieder, 1981).

photosphere (where the altitude is 170 km) to 2×10^3 erg cm^{-2} s^{-1} in the middle chromosphere (where the altitude is 1500 km). The required energy input to heat the middle and upper chromosphere and the corona, which are the regions above the height of 1000 km, is more than 10^5 erg cm^{-2} s^{-1} from Table 1.1. The acoustic energy flux becomes smaller than 10^4 erg cm^{-2} s^{-1} at the bottom of middle chromosphere (at the height of about 1000 km). This implies that,in the solar internetwork regions, the acoustic wave energy dissipates by forming shock waves in the photosphere or in the low chromosphere and is insufficient to heat the middle and upper chromosphere, and the corona.

1.3.2 Magnetic Heating

For heating the solar atmosphere, especially the middle and upper chromosphere, and corona, widely existing magnetic fields were considered to be important. Figure 1.3 shows the plasma beta, which is the ratio of gas pressure to magnetic pressure (given as $\beta = 8\pi p/B^2$, where p is the gas pressure and B is the strength of magnetic field) above an active region (Gary, 2001). The plasma beta model was derived from various observational models of the magnetic field and plasma gas pressure. The magnetic field intensity is given as a function of height between a sunspot of 2500 G and a plage region of 150 G. Plasma β in the photosphere and low chromosphere is in the range almost greater than 0.1. β decreases as the height increases, and becomes smaller than unity in the middle and upper chromosphere and corona (above the height of about 1000 km). This model indicates that the magnetic pressure dominates over the gas pressure in the middle and upper chromosphere, and corona. Although this is the result in the solar active region, it is suggested that, even for the solar quiet region, the dominant heating mechanism is due to the magnetic field because acoustic wave energy dissipates in the solar internetwork regions, which extends from the photosphere to the low chromosphere, before reaching the middle and upper chromosphere, and corona. We focus on the heating mechanisms for inside the magnetic flux tubes.

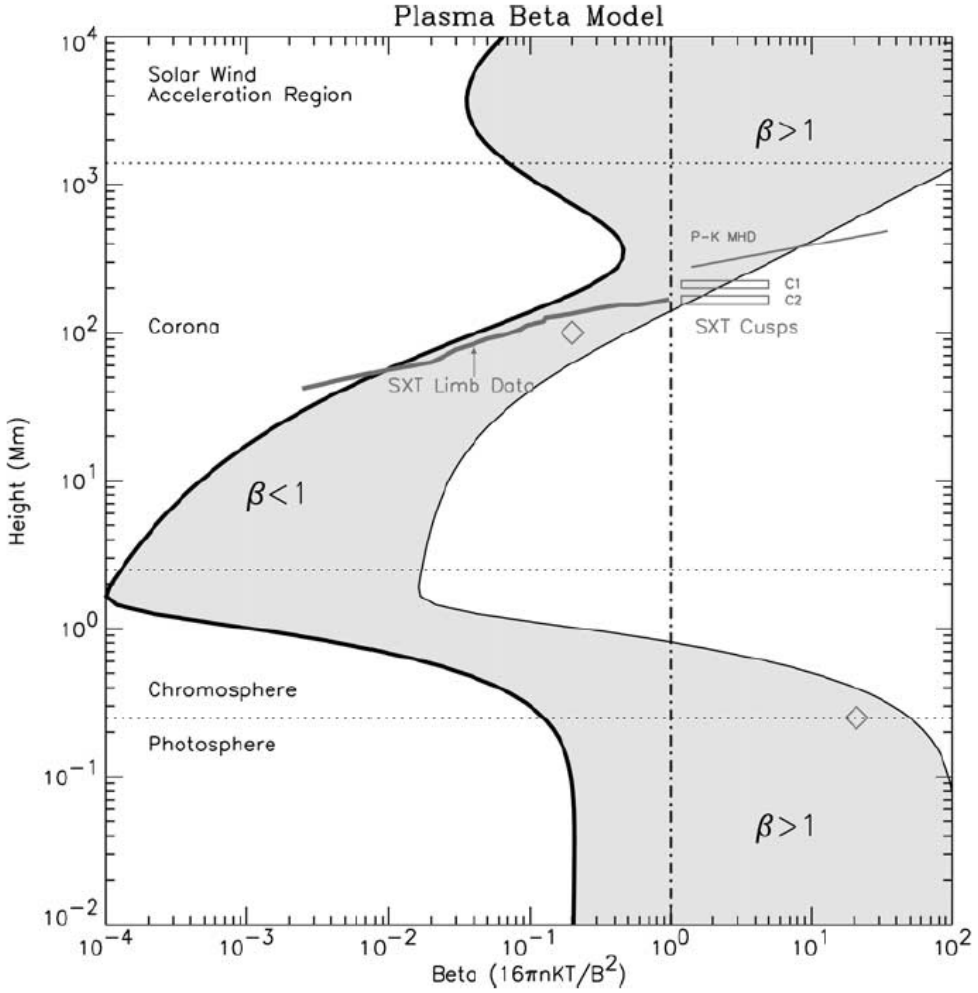

Figure 1.3: Plasma beta model over an active region. The plasma beta is shown shaded for open and closed field lines originating between a sunspot of 2500 G and a plage region of 150 G (Gary, 2001).

There are two possibilities of magnetic heating mechanisms. One is the propagation and dissipation of *magnetohydrodynamic (MHD) waves* and the other is the direct magnetic field dissipation through the magnetic reconnection process. Both MHD waves and magnetic field disturbances for causing the dissipation due to current sheet are generated by the motion of the footpoints of magnetic field lines in the photosphere carried by convection.

For the direct magnetic field dissipation mechanism by the magnetic reconnection, the representative heating theory was proposed by Parker (1972), so called "nanoflare heating". In the theory, the situation in which uniform magnetic fields extend between the two infinite planes was considered. Topology of magnetic field lines is entangled by the random motions of the two plane boundaries. In this case, the field cannot be in magnetostatic equilibrium and the magnetic field discontinuities, which form current sheets, cause dissipation due to the magnetic reconnection. This small scale energy release event is calles as nanoflare. Although many observational signatures of nanoflare have been reported (e.g. Shimizu (1995)), however the statistical results indicate the small energy release event is not enough to heat the corona. The remained possibility is the heating by the numerous number of even smaller energy release event. We cannot deny the possibility of nanoflare heating mechanism unless we detect smaller bright events by means of the observations which have even higher spacial and temporal resolution for the corona and also chromosphere.

In this study, we focus on the heating mechanism due to the propagation and dissipation of MHD waves. In the solar magnetic region, three MHD wave modes (i.e. *fast mode wave*, *slow mode wave*, and *Alfvén wave*) are excited by the turbulent convective motion below the photosphere. The fast magnetoacoustic waves can propagate in any direction, by comparison, the slow mode waves can transmit energy in directions that close to the magnetic field lines. The linear Alfvén waves are incompressible modes, which produces no change in either density or pressure, propagating along the field lines. We are now considering the heating mechanisms inside the magnetic flux tubes in the chromosphere,

and any wave modes have possibilities to heat the layer.

1.4 Alfvén Waves in the Chromosphere

In this thesis, we investigated the propagation and dissipation of Alfvén waves in the chromosphere. Alfvén waves are incompressible wave modes and difficult to form the shock waves, which are thought to carry much energy to the middle chromosphere and above. As mentioned in section 1.3, the principal energy source to heat the solar atmosphere is thought to be the convection below the photosphere. Previous studies suggested that Alfvén waves propagating upwards with wavelength longer than the length scale where the background Alfvén speed changes, which hereafter we call the Alfvénic scale height, may be reflected back, and such a situation might be happened at the boundary between the chromosphere and corona i.e. transition region (Hollweg, 1978; Suzuki & Inutsuka, 2005). It is important to estimate how much wave energy is dissipated or trapped in the chromosphere as waves propagate upwards in order to determine the energy flux going into the corona.

1.4.1 Observations of Transverse Waves

Alfvén waves are incompressible transverse wave modes propagating along magnetic field lines. The observational properties of transverse oscillating motion of magnetic flux tube in the photosphere were reported in Fujimura & Tsuneta (2009). The observation was performed with the spectro-polarimeter of the Solar Optical Telescope (SOT; Tsuneta et al., 2008; Suematsu et al., 2008; Shimizu et al., 2008; Ichimoto et al., 2008) aboard the *Hinode* satellite (Kosugi et al., 2007). The oscillation periods are 3–6 minutes for the pores which are the sunspots lacking penumbrae, and 4–9 minutes for the intergranular magnetic elements. The velocity amplitude of 0.03–0.12 km s^{-1} was found. They analyzed the phase relation between magnetic and velocity fluctuations which are observed simultaneously and suggested that the observed oscillations are corresponding to

the superposition of the upward propagating wave and the downward wave reflected at the boundary between the chromosphere and corona. Even with downward propagating reflected waves, the residual upward Poynting flux was estimated to be 2.7×10^6 erg cm^{-2} s^{-1}, which is in the same order of the required energy flux for heating the quiet chromosphere (shown in Table 1.1). This implies that upward propagating transverse waves in the photosphere have enough large energy to heat the chromosphere.

By observing the chromosphere on the solar limb in optically thick chromospheric lines such as the Balmer lines of Hydrogen (Hα) and resonance lines from singly ionized Calcium (Ca II H and K), it was seen that the chromosphere is filled with sharp jet-like structures ubiquitously. This jet-like phenomena shooting up into the corona is called *spicules*. Figure 1.4 shows an observed image of the solar spicules in Ca II H broad-band filtergraph of SOT. The counterpart features on the solar disk of the solar spicules

Figure 1.4: Spicules at the solar limb taken with with the Ca II H broad-band filtergraph of SOT. A visibility of the image is enhanced by subtracting a background (Suematsu et al., 2008).

are called mottles or fibrils which are dark small structures emanating from small-scale magnetic elements. Many studies have reported the properties of observed solar spicules. The typical width is approximately 1 arcseconds (which is about 700 km) (e.g. Lynch

et al., 1973; Nishikawa, 1988), the mean heights above the photosphere are $10,000$ km and moving upward and downward dynamically within the lifetime of 1–10 minutes, and the moving velocity is about 10–100 km s^{-1}. Dense materials in spicules appear to be moving along the magnetic flux tubes, so we can consider the motion of spicules is representing the topology of the magnetic field lines. The formation mechanism of the solar spicule is unclear. One of the dominant explanation is that interaction between upward propagating shock waves which are formed in the chromosphere and the contact discontinuity at the transition region cause the upward ejection of dense plasma gas, which is observed a spicule.

The presence of transverse waves along spicules have been reported earlier from ground-based observational data (e. g., Zaqarashvili & Erdélyi, 2009). Filtergraph observations with the *Hinode* satellite for the first time clearly resolved small-scale transverse oscillations in spicules (De Pontieu et al., 2007). The properties of transverse waves in a polar coronal hole have been investigated statistically in Okamoto & De Pontieu (2011). It was found that there is a mixture of upward propagating, downward propagating, as well as standing waves along spicules (shown in Figure 1.5). This indicates that the reflection of Alfvén waves at the transition region is sufficiently occurring and the standing waves are formed as a result of the superposition of the upward and downward propagating wave packets. In Figure 1.5, one of the wave packet can be seen to propagate upward with a phase speed which increases with height. The mean phase speed along the whole length of the spicules is 270 ± 30 km s^{-1}. This is roughly consistent with estimates for the Alfvén speed in the quiet chromosphere, where the magnetic field strength is assumed to be 10 G and the plasma number density is of a few times 10^{10} cm^{-3}, so they speculated this is an evidence of propagation of the Alfvén waves in the chromosphere. They also measured the wave periods and amplitudes, and the medians are 45 ± 30 s and 7.4 ± 3.7 km s^{-1}, respectively.

Some other observational studies reported that not only horizontal swaying motions but also twisting torsional motions appear in the solar spicules (Suematsu et al., 2008; De

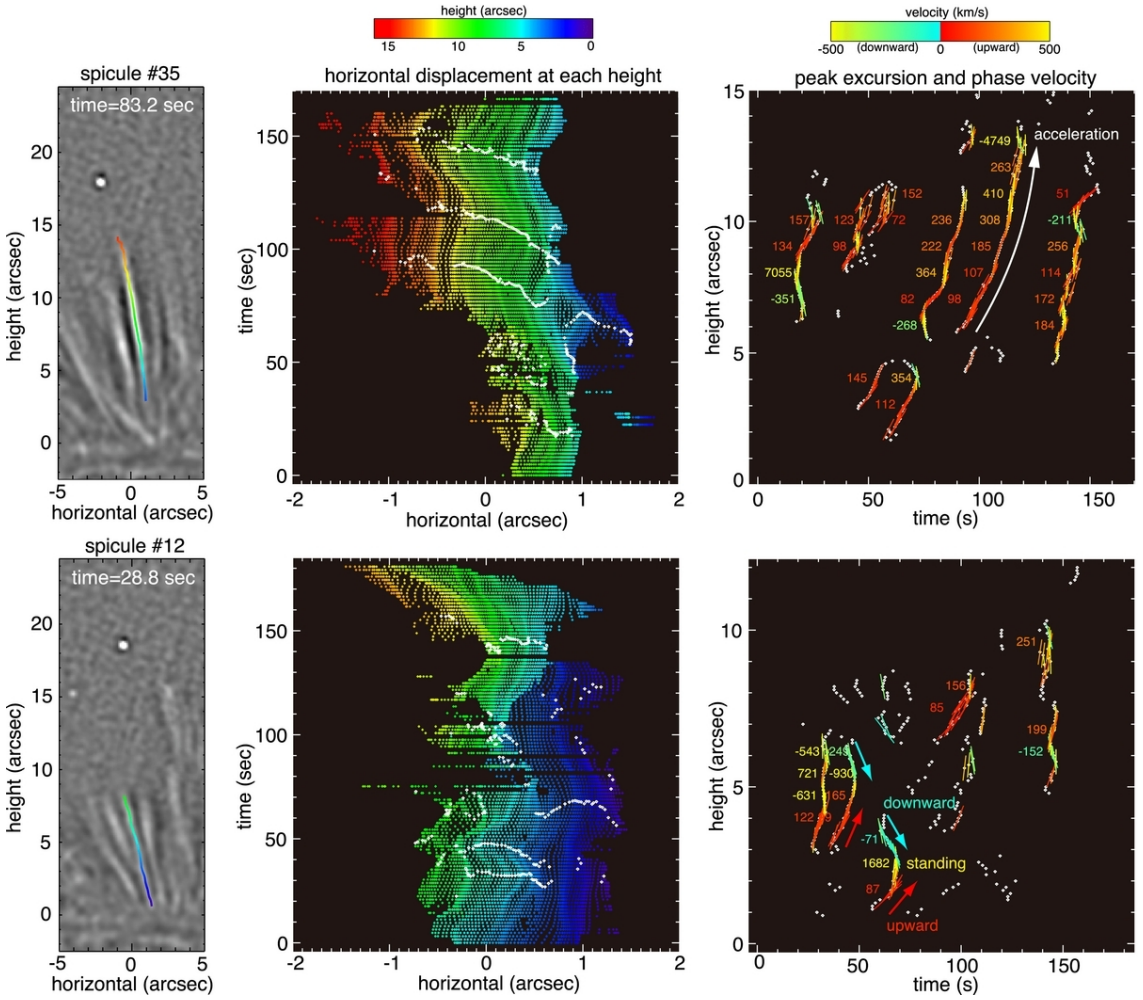

Figure 1.5: Two examples of detected spicules and their transverse displacement. Left panels show the snapshots of detected spicules highlighted with a colored line (whose color is representing the height). Center panels show time variation of horizontal displacements at each height of the spicules. White circular symbols indicate the peak excursions of each wiggle. Right panels show time variation of the height of peak excursions and the phase speed (km s^{-1}). Not only upward propagating waves but also downward propagating waves along spicules can be seen. One of the wave packets in the upper panels is seen to propagate with a phase speed increasing with height. In lower panels, a standing wave is produced as a result of superposition of upward and downward propagating waves (Okamoto & De Pontieu, 2011).

Pontieu et al., 2012, 2014). De Pontieu et al. (2012) analyzed the motions of spicules in the solar limb with spectrograph and imaging spectroscopy. They used data sets obtained with the Swedish 1-m Solar Telescope (SST; Scharmer et al., 2003). They characterized spicules by the simultaneous action of three different types of motions: field-aligned flows of 50–100 km s^{-1}, swaying motions of 15–20 km s^{-1}, and torsional motions of 25–30 km s^{-1}. The swaying and torsional motions are both indicated as signatures of Alfvén waves with periods of order 100–300 s with propagation along spicule axis at phase speeds of order 100–300 km s^{-1}.

1.4.2 Dissipation of Alfvén Waves

Many observational studies have reported the propagation of Alfvén waves in the chromosphere and the measurement of their properties in detail. In terms of the heating mechanism, recent study have reported that the process of dissipation of Alfvén waves detected in the quiet region coronal loops (e.g., Hahn & Savin, 2014). On the other hand, how Alfvén waves dissipate in the chromosphere has not been clear. For solving the chromospheric heating problem, it is considered to be important to investigate the dissipation mechanisms of Alfvén waves in the chromosphere.

1.5 Magnetic Diffusion

The heating mechanisms of the chromosphere by Alfvén waves have been investigated in previous studies theoretically. As the energy dissipation mechanisms of MHD waves, the effects of magnetic diffusion, viscosity, and thermal conductivity are considered to be important in the solar conditions. Khodachenko et al. (2006) investigated the roles of these mechanisms in the chromosphere and concluded that, for the Alfvén waves, the dissipation due to the *magnetic diffusion* is more important than viscosity and thermal conductivity. In this thesis, for the dissipation mechanisms of Alfvén waves, we focus on the damping of waves caused by magnetic diffusion.

1.5.1 The Effect of Neutrals

It is known that the chromosphere has relatively lower temperature ($T \sim 10^4$ K) than the corona ($T \sim 10^6$ K) and the ionization degree in the chromosphere becomes smaller. The ionization degree of hydrogen along the height is given from VAL-C model in Vernazza et al. (1981). At zero point of height, the ionization degree of hydrogen is about 10^{-3}. The ionization degree decreases to about 10^{-4} at the height of temperature minimum 500 km. From that height, the ionization degree rises as the height increases and becomes almost unity from above the height of 2000 km,

The presence of neutrals leads to break the approximation of the ideal MHD. Because of the collisions between neutrals and ionized plasmas cause additional effects, such as *Hall effect* and *ambipolar diffusion*. The ambipolar diffusion term is sometimes referred as "ion-neutral collision term", which causes the magnetic diffusion due to collisions between neutral and charged components being frozen-in into the magnetic field. Hall effect appears as a result of the different drift velocities of electrons and ions, which are not equally affected neutrals.

1.5.2 MHD Waves in Partially Ionized Plasmas

The propagation of MHD waves in partially ionized plasmas have been investigated in many previous studies. Osterbrock (1961) presented an analysis of damping rates of linear MHD waves in the chromosphere due to charged particle-neutral collisions and a scalar viscosity. He concluded that damping of MHD waves is not important for the chromospheric heating. However, he used magnetic field strengths orders of magnitude smaller than recent observational values ($B = 0.5, 2, 50$ G). This may affect the magnetic diffusivity due to the collision between charged particle and neutral.

The 1.5D analytical models for damping of Alfvén waves in the partially ionized chromosphere have been developed in De Pontieu & Haerendel (1998) and De Pontieu et al. (2001). They estimated the damping rate and found that the damping of upward

propagating Alfvén waves with frequencies in the range between 0.1–1.0 Hz can cause not only significant heating in the chromosphere but also upward motion of the upper chromospheric plasma, which can sustain an already formed spicule dynamically and thermodynamically. This type of support of spicule previously has been suggested in Haerendel (1992). Leake et al. (2005) presented one-dimensional not only analytic but also numerical MHD models of Alfvén wave damping in the strongly magnetized region of the chromosphere. The models assume a background atmosphere given by VAL-C model (Vernazza et al., 1981, shown in Figure 1.1). They used the generalized Ohm's law derived in Braginskii (1965). This study supports the main results of De Pontieu & Haerendel (1998) and De Pontieu et al. (2001), but the models in Leake et al. (2005) do not include the low chromosphere and the photosphere (below the height of 1000 km).

Kazeminezhad & Goodman (2006) has presented 1.5D nonlinear MHD simulation and compute the heating rate due to dissipation of Alfvén waves. The background atmosphere is assumed to be given by model CM of Fontenla, Avrett, and Loeser, so called FAL model. It is essentially the model used in Fontenla et al. (2002). They suggested that the waves are almost completely damped out in the chromosphere by the time in which the wave propagates a distance of one wavelength. They focus on the middle and upper chromosphere, and the photosphere and low chromosphere are excluded in this simulation. The waves are initiated at the bottom of the middle chromosphere (at the height of 1000 km). They used a constant vertical magnetic field ($B_z = 25$ G). The smaller magnetic field strength means that the background Alfvén speed is smaller. If the Alfvén waves propagate slowly, these waves experience more dissipation in the chromosphere.

Goodman (2011), which presented the result of more realistic case than that in Goodman & Kazeminezhad (2010). The conditions for linear, non-plane Alfvén waves driven in the photosphere to give significant chromospheric heating rate that is comparable to the chromospheric radiative loss ($\sim 10^6$ erg cm^{-2} s^{-1}, shown in Table 1.1) is estimated. They concluded that the oscillations drive a chromospheric heating flux of 10^7–10^8 erg cm^{-2} s^{-1} at frequencies ~ 0.1–1.0 Hz for background magnetic field strengths $B \geq 700$ G and

magnetic field perturbation amplitude ~ 0.01–$0.1B$. In their result, most heating occurs in the photosphere due to the classical ohmic diffusion and this regulates the Poynting flux into the chromosphere. In the upper chromosphere, heating due to the ambipolar diffusion becomes effective.

The studies above (Kazeminezhad & Goodman, 2006; Goodman, 2011) assume a constant background magnetic field. In the solar atmosphere, the magnetic field has a topology of open magnetic flux tube (e.g., Gabriel, 1976) and has decreasing strength with height. Moreover, the magnetic field strength in Goodman (2011) is relatively strong. The weaker magnetic field strength might affect heating rate due to the ambipolar diffusion term.

1.6 Nonlinear Effect of Alfvén Waves

As another possible mechanism to cause the dissipation of Alfvén waves, the nonlinear coupling of waves was considered. Due to the gradient of magnetic pressure associated with propagation of nonlinear Alfvén waves, compressible MHD wave modes can be excited. These excited compressible waves also steepen to form shock waves and dissipate in the solar atmosphere. The nonlinear mode conversion process of Alfvén waves has been investigated in various studies (Hollweg et al., 1982; Hollweg, 1982; Kudoh & Shibata, 1999; Suzuki & Inutsuka, 2005, 2006; Matsumoto & Shibata, 2010).

Hollweg et al. (1982) studied the evolution of low frequency nonlinear Alfvén wave pulses launched from the photosphere and propagating on open magnetic flux tubes by numerical MHD simulations for the first time. They assumed the vertical and rigid flux tube. It is shown that Alfvén waves can steepen into fast mode shocks in the chromosphere, which move the transition region upward and heat the upper chromosphere and corona. However, the structures of formed spicules were too short and cool. Kudoh & Shibata (1999) studied the effect of randomly generated Alfvén waves in the photosphere. They found that spicules with height of observed value (which is higher than 5000 km)

could be generated. In their model, the initial velocity amplitude in the photosphere was set to be greater than 1 km s^{-1}.

Matsumoto & Shibata (2010) included a realistic horizontal velocity spectrum as a wave generator in the MHD simulations. They derived a temporal spectrum of the photospheric motion from *G*-band movies of *Hinode*/SOT. Figure 1.6 shows their power spectral density. They showed that the total energy flux at the corona becomes larger and the

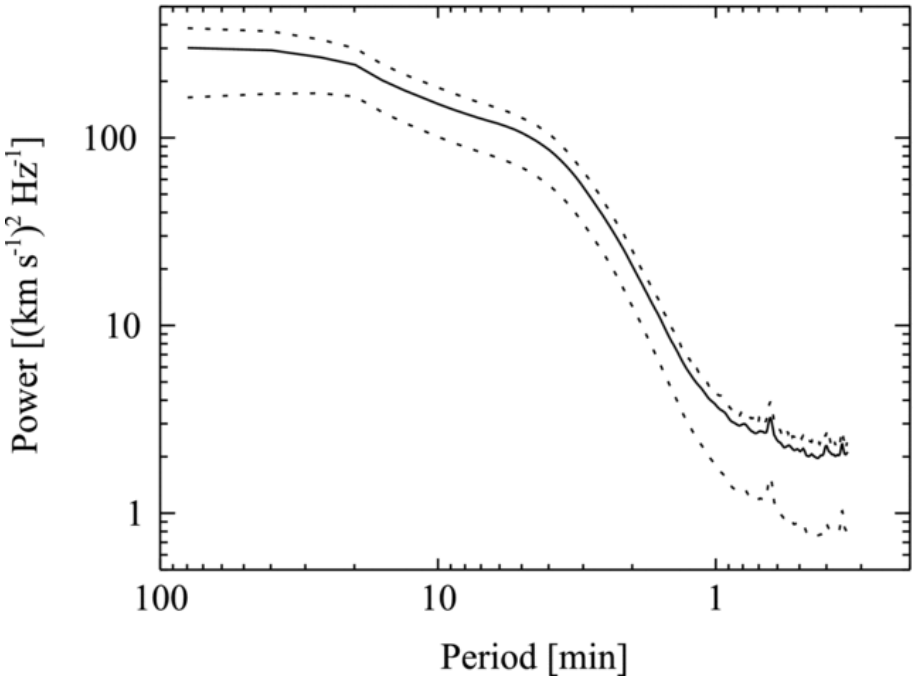

Figure 1.6: Power spectral density of photospheric horizontal velocity. After the horizontal velocity is derived from observational data sets, the spectrum is estimated by fast Fourier transform (FFT). The solid line shows the mean power and dotted lines represent 1σ (Matsumoto & Shibata, 2010).

transition region's height becomes higher in the case using the observed spectrum than the white or pink random noise spectrum as a wave generator. By performing Fourier analysis, they found that this region becomes a wave resonant cavity and has at least three resonant frequencies at 1, 3 and 5 mHz in their model. The photospheric boundary is set as a fixed one while the transition region works as a free boundary because of the high Alfvén speed in the corona. In this situation, the resonance occurs between the photosphere as a node and the transition region as an antinode. However, a reflective boundary condition at

the photosphere is based on the assumption that Alfvén speed under the photosphere may be smaller than in the upper atmosphere and the flux tube can be easily bent by convection motion. This assumption may not be valid if the magnetic flux tube is strong enough and extends straight down below the photosphere. It is important to estimate how much wave energy penetrates down into the convection zone under the photosphere.

The propagation of nonlinear Alfvén waves on vertically open magnetic flux tube including the effect of magnetic diffusion due to the collisions between charged particles and neutrals has been studied by James et al. (2003) and Erdélyi & James (2004). The used velocity amplitude is relatively larger than values taken from observations, and, even in their models, the penetration of waves into the convection zone below the photosphere has not been investigated.

1.7 Aim of This Study

Fundamental motivation of this study is investigating the propagation of Alfvén waves along a vertically open magnetic flux tube in the partially ionized chromosphere. As a heating mechanism which provides sufficient energy to not only the photosphere and low chromosphere but also middle and upper chromosphere, and corona, the dissipation mechanisms of incompressible Alfvén waves are considered because pure compressible waves easily form shocks and dissipate in the photosphere and low chromosphere.

Collision between charged particles and neutrals cause additional magnetic diffusion, so called ambipolar diffusion in the chromosphere and damping of Alfvén wave occurs effectively. On the other hand, nonlinear Alfvén waves can be converted into compressional MHD wave modes. Shock dissipation of these wave modes is also thought to contribute to heat the chromosphere. However, the effect of magnetic diffusion to nonlinear propagation of Alfvén waves has not been studied enough. Damping of Alfvén waves by magnetic diffusion may reduce the nonlinearity of waves. The properties of waves propagating in the chromosphere, such as amplitudes or frequencies should be consistent

with the observational values. These are summarized in Figure 1.7

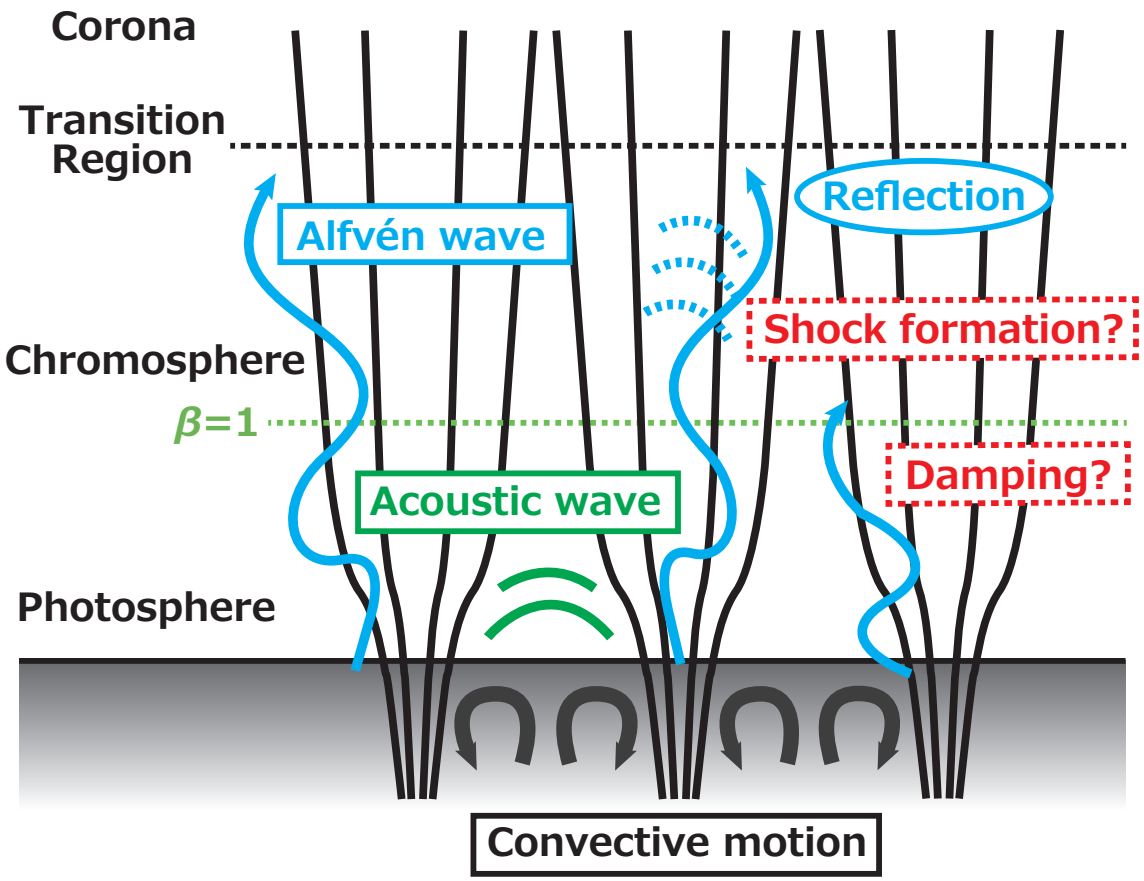

Figure 1.7: Schematic drawing of the propagation and dissipation of waves in the chromosphere.

In this thesis, the effect of magnetic diffusion to Alfvén waves propagating along open magnetic flux tube from the convection zone to the corona is investigated in both analytic and numerical ways. In Chapter 2, we give analytic estimates of the effect of magnetic diffusion to nonlinear propagation of Alfvén waves and suggest that reflection at boundaries of the chromosphere is important for the chromospheric heating. In Chapter 3, we describe our model and initial settings of 1.5D numerical MHD simulation. In Chapter 4, we present the result of simulation. In Chapter 5, a discussion is given. A summary of this thesis and future works are given in Chapter 6.

Chapter 2

Estimates

In this chapter, first of all we estimate the effect of magnetic diffusion by carrying out simple analytic calculation. To investigate the effect of magnetic diffusion to the process of shock formation of nonlinear Alfvén waves, we calculate damping length by magnetic diffusion and propagation length to form shock wave of a wave driven at the bottom of the photosphere.

2.1 Damping Length by Magnetic Diffusion

The damping of upward propagating magnetic waves is caused by magnetic diffusion mechanisms (which are classical ohmic diffusion and ambipolar diffusion), Although viscosity and thermal conduction also cause the damping of waves, here we neglect these effects because the magnetic diffusion is more important for the energy dissipation of Alfvén waves in the chromosphere (Khodachenko et al., 2006). For a wavelength λ, the time scale for magnetic diffusion is simply given as

$$\tau_d = \frac{\lambda^2}{\eta}, \tag{2.1}$$

where η is the magnetic diffusivity. The distance that an Alfvén wave can propagate before it dissipates, so called *damping length* is

$$L_d = c_A \tau_d = \frac{1}{\eta} \frac{{c_A}^3}{f^2}, \tag{2.2}$$

where f ($= c_A/\lambda$) is the wave frequency.

In order to calculate magnetic diffusion coefficients, we follow derivation in Khomenko & Collados (2012). For simplicity, we consider a hydrogen plasma with three components: hydrogen ions (i), hydrogen neutrals (n), and electrons (e), and assume elastic collisions and no chemical reactions in the system. The generalized Ohm's law is given from Braginskii (1965):

$$\boldsymbol{E} + \frac{1}{c}\, \boldsymbol{v} \times \boldsymbol{B} = \eta_O \boldsymbol{J} + \eta_H \left[\boldsymbol{J} \times \boldsymbol{e_B}\right] + \eta_A \left[\boldsymbol{e_B} \times (\boldsymbol{J} \times \boldsymbol{e_B})\right], \tag{2.3}$$

where v is center of the mass velocity of the system, $\boldsymbol{e_B}$ a unit vector along the magnetic field line. This form of the generalized Ohm's law neglects the temporal variations of the relative ion-neutral velocity, the effect on the currents by the partial pressure gradients of the three species (electrons, ions, and neutrals), and the gravity force acting on electrons. The diffusion coefficients are defined, by means of the resistivity η_α (where $\alpha = O$, H, A), as $\tilde{\eta}_\alpha = \eta_\alpha\, c^2/4\pi$. Each of coefficients is given by the following formulae

$$\tilde{\eta}_O = \frac{c^2}{4\pi} \frac{m_e^2 \left(\nu_{ei} + \nu_{en}\right)}{e^2 \rho_e} \tag{2.4}$$

$$\tilde{\eta}_H = \frac{c}{4\pi} \frac{m_e |B|}{e \rho_e} \tag{2.5}$$

$$\tilde{\eta}_A = \frac{1}{4\pi} \frac{\left(\rho_n/\rho\right)^2 |B|^2}{\left(\rho_i \nu_{in} + \rho_e \nu_{en}\right)}. \tag{2.6}$$

Here m_e is the mass of electron, ρ_α (where $\alpha = e$, i, n) the mass density of each particle, $\rho = \rho_e + \rho_i + \rho_n$ the total mass density, and $\nu_{\alpha\beta}$ (where α and β take e, i, or n) are collisional frequencies. Three terms on the right hand side of the generalized Ohm's law

(equation (2.3)) are the ohmic term, the Hall term, and the ambipolar term. The diffusion coefficients are given if the collisional frequency, the magnetic field strength, and the neutral fraction are determined. In order to estimate these values in the chromosphere, we assume the temperature distribution almost the same as VAL-C in Vernazza et al. (1981), and the atmosphere to be in hydrostatic equilibrium. The height of transition region is located at 2100 km above the bottom of the photosphere. The ionization degree of hydrogen is also assumed to be almost the same as VAL-C model. The atmospheric conditions are shown in Figure 2.1. Since we are interested in the effect of magnetic diffusion along an open magnetic flux tube, the magnetic field strength is set to decrease with height, from about 1500 G in the photosphere to 50 G in the corona. For calculating the magnetic field strength, We assume that the plasma beta is unity and constant with height. The formula of frequencies for collision between charged particles is given from Braginskii (1965), and the formulae for collision between charged particles and neutrals are given from De Pontieu & Haerendel (1998):

$$\nu_{ei} = \frac{4\sqrt{2\pi}\Lambda e^4 n_e}{3\sqrt{m_e}(k_B T)^{3/2}} \tag{2.7}$$

$$\nu_{en} = n_n \sqrt{\frac{8k_B T}{\pi m_{en}}}\sigma_{en} \tag{2.8}$$

$$\nu_{in} = \frac{n_n}{2}\sqrt{\frac{8k_B T}{\pi m_{in}}}\sigma_{in}, \tag{2.9}$$

where Λ is the Coulomb logarithm calculated in Braginskii (1965) as

$$\Lambda = \begin{cases} 23.4 - 1.15\log_{10} n_e + 3.45\log_{10} T & (T < 50 \text{ eV}) \\ 25.3 - 1.15\log_{10} n_e + 2.3\log_{10} T & (T > 50 \text{ eV}) \end{cases} \tag{2.10}$$

with n_e expressed in cgs unit and T is in eV, $m_{en} = m_e m_n/(m_e + m_n)$ and $m_{in} = m_i m_n/(m_i + m_n)$, and the respective cross sections are $\sigma_{en} = 10^{-15}$ cm^2 and $\sigma_{in} = 5 \times 10^{-15}$ cm^2. The results of calculation of magnetic diffusion coefficients are given in Figure 2.2. In the low photosphere (below the height of 200 km), the magnetic diffusivity

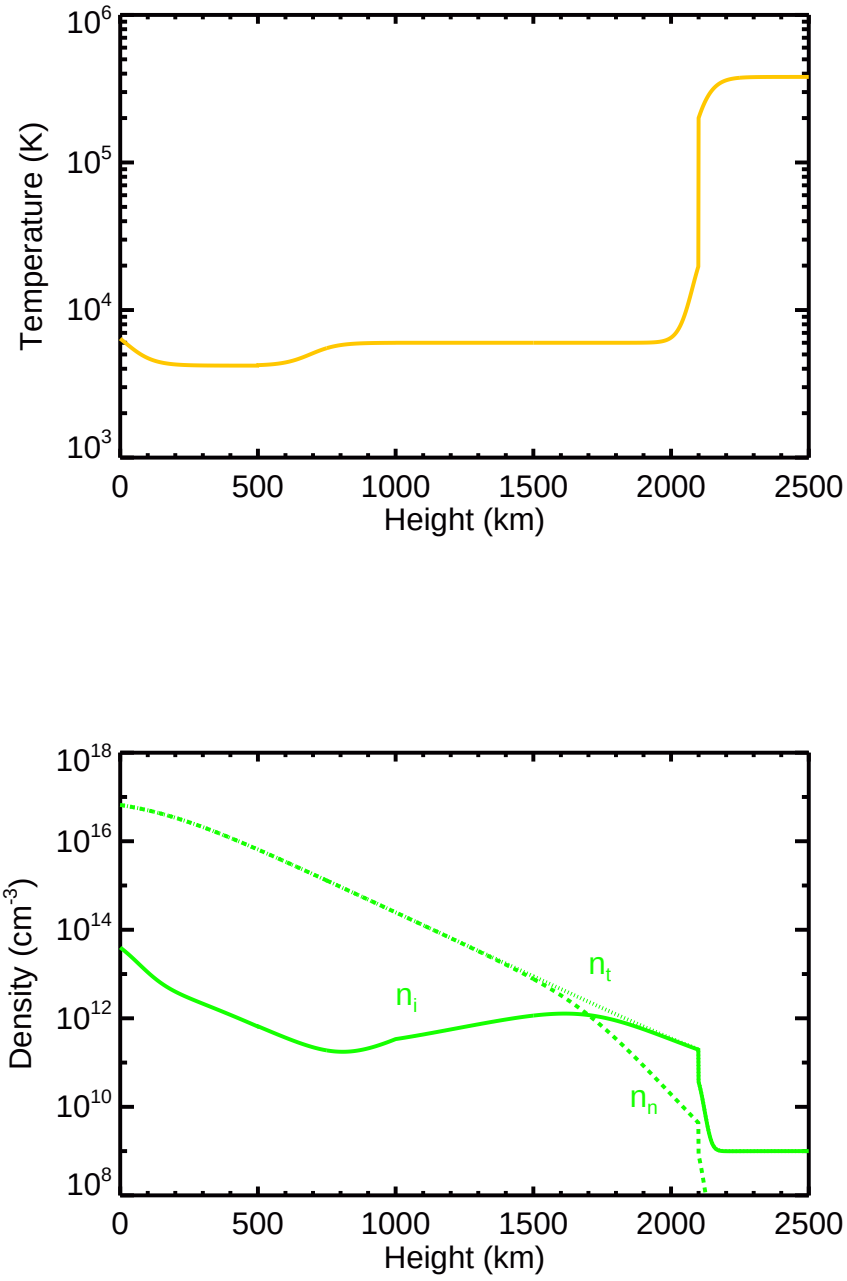

Figure 2.1: The atmospheric models we used to calculate the magnetic diffusivity, which are assumed from VAL-C model in Vernazza et al. (1981). The top and bottom panels show the temperature and density distributions, respectively. In the bottom panel, the solid line shows the distribution of number density of the hydrogen ions (n_i), and the dashed line shows that of hydrogen neutrals (n_n). The total number density ($n_t = n_e + n_i + n_n$) is shown in dotted line, where $n_e (= n_i)$ is the number density of electrons.

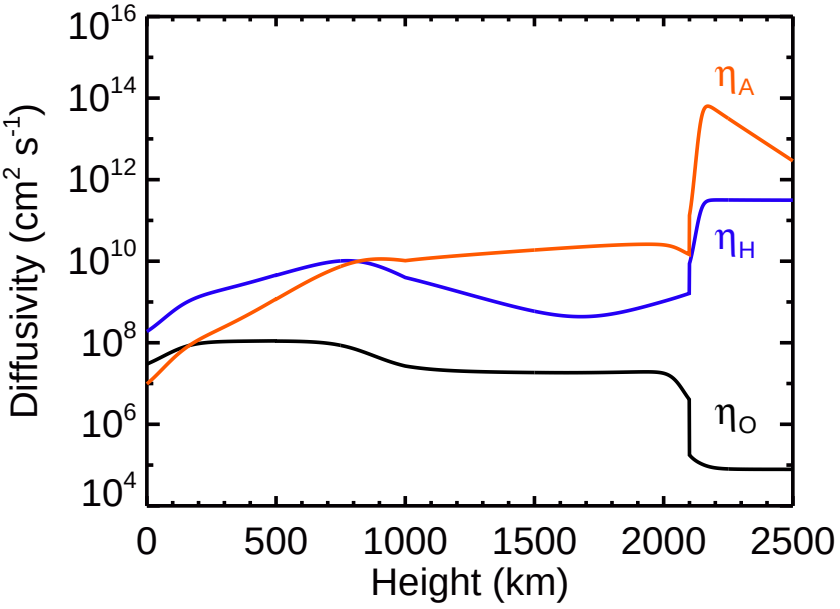

Figure 2.2: Magnetic diffusion coefficients from equation (2.3) calculated in the model atmosphere representing an open magnetic flux tube. The black, blue and red lines show the magnetic diffusion coefficients $\tilde{\eta}_O$, $\tilde{\eta}_H$ and $\tilde{\eta}_A$, respectively.

is stronger in the order of the Hall term, ohmic term, ambipolar term. The ambipolar term increases with height. From the middle of the photosphere (where the height of 200 km), the ambipolar term becomes larger than the ohmic term and dominant over the other terms from the height of 1000 km.

The Joule heating rate due to the magnetic diffusion is calculated by using the generalized Ohm's law in Khomenko & Collados (2012) and written as

$$\begin{aligned} q &= \boldsymbol{J} \cdot \left[\boldsymbol{E} + \frac{1}{c} \boldsymbol{u} \times \boldsymbol{B} \right] \\ &= \eta_O \boldsymbol{J}^2 + \eta_A \left[\boldsymbol{e_B} \times (\boldsymbol{J} \times \boldsymbol{e_B}) \right]^2 . \end{aligned} \tag{2.11}$$

As can be seen, the Hall term does not appear in the equation of heating rate due to the magnetic diffusion. This can be understood that the diffusion coefficient of the Hall term $\tilde{\eta}_H$ does not depend on the collisional frequencies. Since we are interested in the effect of

magnetic diffusion for the chromospheric heating mechanism, in following analysis, we will neglect the effect of the Hall term.

In order to calculate damping length from equation (2.2), the magnetic diffusivity, Alfvén speed and wave frequency f are required. The total magnetic diffusivity is approximately given as $\eta = (\eta_O + \eta_A)c^2/4\pi$. In stratified atmospheric model, Alfvén speed $c_A = B_0/\sqrt{4\pi\rho}$ (where B_0 is the background magnetic field strength) increases with height. We give the wave frequency f as a parameter. The range of wave frequency which has enough power to heat the chromosphere is indicated from the power spectrum calculated from the observed horizontal velocity in the photosphere, which was given in Matsumoto & Shibata (2010) (shown in Figure 1.6). From the power spectrum, the r.m.s. velocity of wave frequencies at $f = 10^{-3}, 10^{-2}, 10^{-1}$ Hz is calculated all as 0.1–1.0 km s^{-1} and the energy flux is $\sim 10^8$ erg cm^{-2} s^{-1}, so waves with these frequencies have possibility to heat the upper solar atmosphere. In the case of wave frequencies at $f = 10^{-3}, 10^{-2}, 10^{-1}$ Hz, the variation of damping length with height is shown in Figure 2.3. The damping lengths of any frequencies are $> 10^6$ km, which are much larger than the thickness of the chromosphere ~ 2000 km.

2.2 Shock Formation Length

We are interested in the effect of magnetic diffusion to the production of compressible MHD waves from the Alfvén waves by the nonlinear effect. In order to investigate this, we calculate the distance that Alfvén waves can propagate before forming shock waves by exciting the compressible waves, which we call the shock formation length. Wentzel (1977) proposed that the shock formation length for waves of wavenumber k generating a density perturbation ρ_1 can be written in order of magnitude as $d = \rho/(k\rho_1)$. The density perturbation produced by Alfvén waves is estimated as $\rho_1/\rho \sim (v_1/c_A)^2$, where v_1 is the

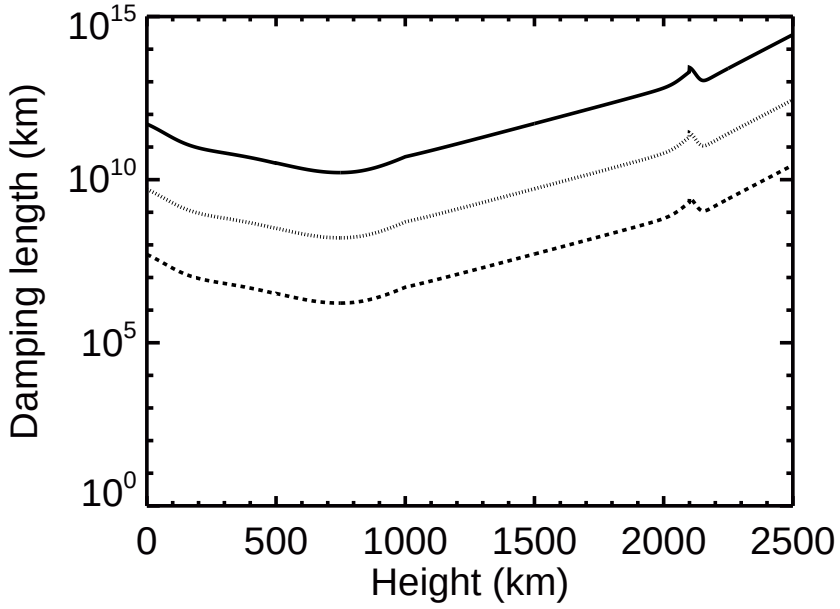

Figure 2.3: Variation of damping length by magnetic diffusion. The solid, dotted, dashed lines show the results of wave frequencies at $f = 10^{-3}, 10^{-2}, 10^{-1}$ Hz, respectively.

velocity amplitude of Alfvén wave. The shock formation length becomes

$$L_s \sim \frac{c_A}{f}\left(\frac{c_A}{v_1}\right)^2. \tag{2.12}$$

If we set the initial velocity amplitude v_1 of an upward propagating Alfvén wave from the bottom of the photosphere, we can estimate the variation of v_1 with respect to the height by assuming that the Pynting flux $\rho v_1^2 c_A$ is conserved. By using the same atmospheric models as those in section 2.1, we calculate the variation of the shock formation length at each height. The results where the initial velocity amplitudes are set as $v_1 = 1.0$ km s^{-1} and $v_1 = 0.1$ km s^{-1} are shown in Figure 2.4. If the initial velocity amplitude is set as $v_1 = 1.0$ km s^{-1}, the shock formation lengths become 10^6, 10^5, 10^4 km at minimum for the waves with frequencies at $f = 10^{-3}$, 10^{-2}, 10^{-1} Hz, respectively. The results of the velocity amplitude $v_1 = 0.1$ km s^{-1} show much longer shock formation lengths, which are larger than about 10^6 km. This is almost comparable to the minimum damping length

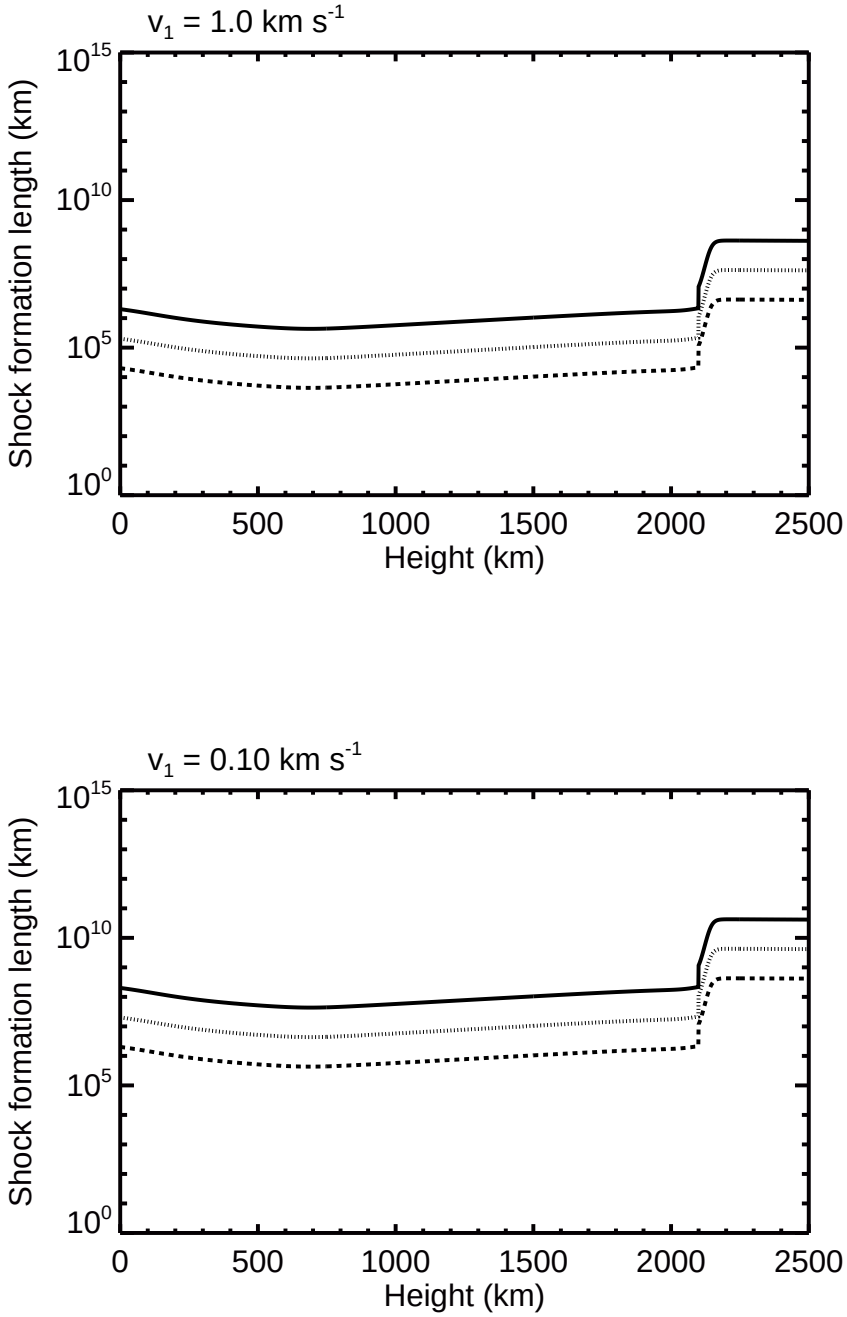

Figure 2.4: Variation of the shock formation length. The top panel shows the results of the initial velocity amplitude $v_1 = 1.0$ km s^{-1} and the bottom shows those of $v_1 = 0.1$ km s^{-1}. The solid, dotted, dashed lines show the results of wave frequencies at $f = 10^{-3}, 10^{-2}, 10^{-1}$ Hz, respectively.

by the magnetic diffusion for wave frequency $f = 10^{-1}$ Hz (which is shown in Figure 2.3). As a result, the shock formation length becomes smaller than or comparable to the damping length, however, it is larger than the thickness of the chromosphere (~ 2000 km).

2.3 Comparison of Length Scales

From the simple estimation, both the damping length and shock dissipation length are larger than the thickness of the chromosphere (~ 2000 km). If the vertical open magnetic flux tube is considered, upward propagating Alfvén wave can reach the transition region height before the dissipation sufficiently occurred, and most of waves may be reflected. Moreover, in order to heat the chromosphere by the dissipation of Alfvén wave, it is important that the reflection at the photosphere occurs and the Alfvén waves are trapped inside the chromosphere.

Chapter 3

Method

In Chapter 2, we suggested the importance of investigating the propagation and reflection of Alfvén waves in the chromosphere. For investigation of the nonlinear propagation of Alfvén waves in the chromosphere, performing numerical simulation becomes powerful tool and we can calculate the reflection rate of Alfvén waves at the boundaries of the chromosphere from the simulation results. In this chapter, we present the numerical settings, such as solving equations and initial conditions.

3.1 Basic Equations

We follow the settings in Hollweg et al. (1982). A rigid, vertical, axisymmetric and initially untwisted magnetic flux tube is assumed. A local orthogonal curvilinear coordinate system (x, y, z) is defined, where x is the distance along a poloidal magnetic field line, y the azimuthal angle measured around the rotation axis of the flux tube, z a coordinate measured in the $\hat{x} \times \hat{y}$ direction (where $\hat{x}$ and $\hat{y}$ are unit vectors in the x and y directions, respectively). The condition of axial symmetry is written as

$$\frac{\partial}{\partial y} = 0. \tag{3.1}$$

We use the 1.5-dimensional approximation, so motions and gradients perpendicular to the magnetic flux tube are suppressed as

$$\frac{\partial}{\partial y} = 0, \ \frac{\partial}{\partial z} = 0, \ v_z = 0, \ B_z = 0, \tag{3.2}$$

where v_z and B_z are the velocity and the magnetic field perpendicular the poloidal magnetic field, respectively, and the velocity in the azimuthal angle direction v_y and the magnetic field B_y are taken into account. In z direction, the horizontal homogeneity is assumed and the motions in this direction are suppressed. This assumption is valid if the magnetic field lines are close to the flux tube axis and the flux tube is approximately vertical. Figure 3.1 shows the schematic drawing of the assumed magnetic flux tube and coordinate system.

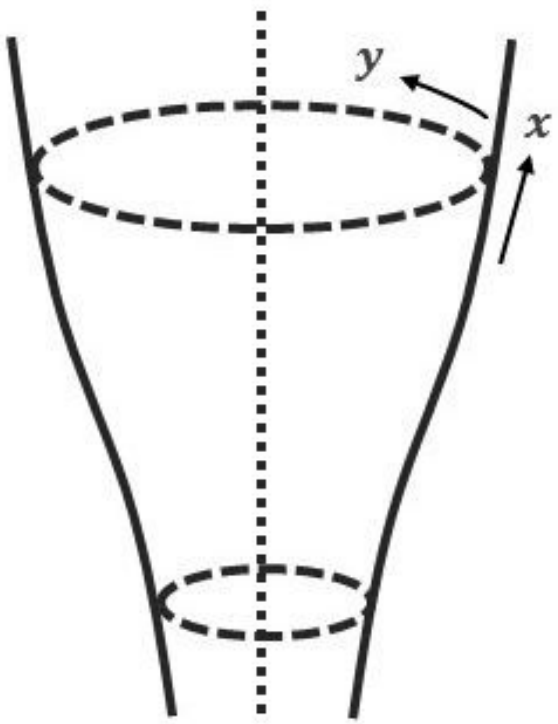

Figure 3.1: Schematic drawing of assumed local orthogonal curvilinear coordinate system in this numerical settings. Solid lines show the magnetic field line and a dotted line is the flux tube axis.

Here we consider the ideal compressible MHD including gravity in the system. Thermal conduction, radiative cooling, viscosity, and resistivity are not considered in our calculations. For simplicity, the effect of the curvature of magnetic field line is neglected. The basic MHD equations are as follows: mass conservation,

$$\frac{\partial}{\partial t}\left(\rho S\right)+\frac{\partial}{\partial x}\left(\rho v_x S\right)=0; \tag{3.3}$$

the x component of the momentum equation,

$$\frac{\partial}{\partial t}\left(\rho v_x S\right)+\frac{\partial}{\partial x}\left[\left(\rho v_x^2+p+\frac{B_y^2}{8\pi}\right)S\right]=-\rho g S+\left(p+\frac{B_y^2}{8\pi}\right)\frac{dS}{dx}; \tag{3.4}$$

the y component of the momentum equation,

$$\frac{\partial}{\partial t}\left(\rho v_y S\right)+\frac{\partial}{\partial x}\left[\left(\rho v_x v_y-\frac{B_x B_y}{4\pi}\right)S\right]=0; \tag{3.5}$$

the y component of the induction equation,

$$\frac{\partial}{\partial t}\left(B_y S\right)+\frac{\partial}{\partial x}\left[\left(v_x B_y-v_y B_x\right)S\right]=0; \tag{3.6}$$

the adiabatic energy equation,

$$\begin{aligned}\frac{\partial}{\partial t}\left[\left(\frac{p}{\gamma-1}+\frac{1}{2}\rho v^2+\frac{B_y^2}{8\pi}\right)S\right] &+ \frac{\partial}{\partial x}\left[\left(\left(\frac{\gamma}{\gamma-1}p+\frac{1}{2}\rho v^2+\frac{B_y^2}{4\pi}\right)v_x-\frac{B_x B_y}{4\pi}\right)S\right] \\ &= -\rho g v_x S;\end{aligned} \tag{3.7}$$

where S is the cross section of the flux tube, ρ the mass density, p the gas pressure, v_x the velocity along the magnetic field and $v=\sqrt{v_x^2+v_y^2}$, B_x the poloidal component of the magnetic field, g the gravitational acceleration, which is assumed to be constant (given as $g=2.7\times10^4$ cm s^{-2}), and γ the ratio of specific heats is assumed to be $\gamma=5/3$.

Temperature is derived from the equation of state:

$$T = \frac{m_p}{k_B}\frac{p}{\rho}, \tag{3.8}$$

where m_p is the mass of proton ($m_p = 1.7 \times 10^{-24}$ g), k_B the Boltzmann's constant, and the mean molecular weight is assumed to be 1 and constant.

3.2 Initial Conditions

3.2.1 Atmospheric Conditions

Our numerical domain ranges from the convection zone to the corona, which is given as $x \in [-L, L]$ and $L = 10^5$ km, since we are interested in the reflection of Alfvén waves at the top and bottom boundaries of the chromosphere. The position of $x = 0$ is located at the surface of the convection zone which is corresponding to the bottom of the photosphere.

The initial temperature distribution above the photosphere (where $x \geq 0$) is taken to be as follows:

$$T(x) = T_0 + (T_{\text{cor}} - T_0)\left[\frac{1}{2}\left(\tanh\left(\frac{x - x_{\text{tr}}}{w_{\text{tr}}}\right) + 1\right)\right], \tag{3.9}$$

where T_0 is the temperature at $x = 0$, which is assumed to be 5000 K, T_{cor} the coronal temperature (10^6 K), x_{tr} the height of transition region (at 2500 km), and w_{tr} the width of transition region is assumed to be 100 km. In a whole region, the stratified condition is assumed, which is determined by solving the equation of hydrostatic equilibrium:

$$\frac{dp}{dx} = -\rho g, \tag{3.10}$$

under the given constant gravity distribution. The density at $x = 0$ is assumed to be

1.7×10^{-7} g cm^{-3}. In the convection zone (where $x \leq 0$), it is assumed that the adiabatic condition can be applied as

$$\frac{p}{\rho^{\gamma}} = \text{contant.} \tag{3.11}$$

The initial velocity field along the magnetic field is assumed to be $v_x = 0$. By solving these equations, we get the initial atmospheric condition, which is showed in Figure 3.2.

3.2.2 Condition of Magnetic Flux Tube

In our calculations, x component of magnetic field does not change with time, so we do not solve the time evolution. The spatial distribution is determined from the initial distribution of pressure as below:

$$B_x = \sqrt{\frac{1}{\beta} 8\pi p}, \tag{3.12}$$

where p is the pressure and β is the plasma beta at $t = 0$. As a representative case, we set a plasma beta distribution assumed from the model in Gary (2001) which is shown in Figure 1.3. Since we focus on the region inside the magnetic flux tube, the plasma beta is set to be small in the range of the model in Gary (2001). We set the plasma beta to be unity below the low chromosphere (where $x < 1000$ km) and decrease to $\beta = 0.1$ in the corona. We call this case as Case (I). The distributions of plasma beta, x component of magnetic field which is calculated from equation (3.12), and the background Alfvén speed (which is calculated as $c_A = B_x/\sqrt{4\pi\rho}$) are shown in Figure 3.3.

The distribution of the cross section of magnetic flux tube is determined from that of B_x by using following condition:

$$SB_x = \text{constant}, \tag{3.13}$$

where the right hand side of the equation is chosen to be unity in our calculations.

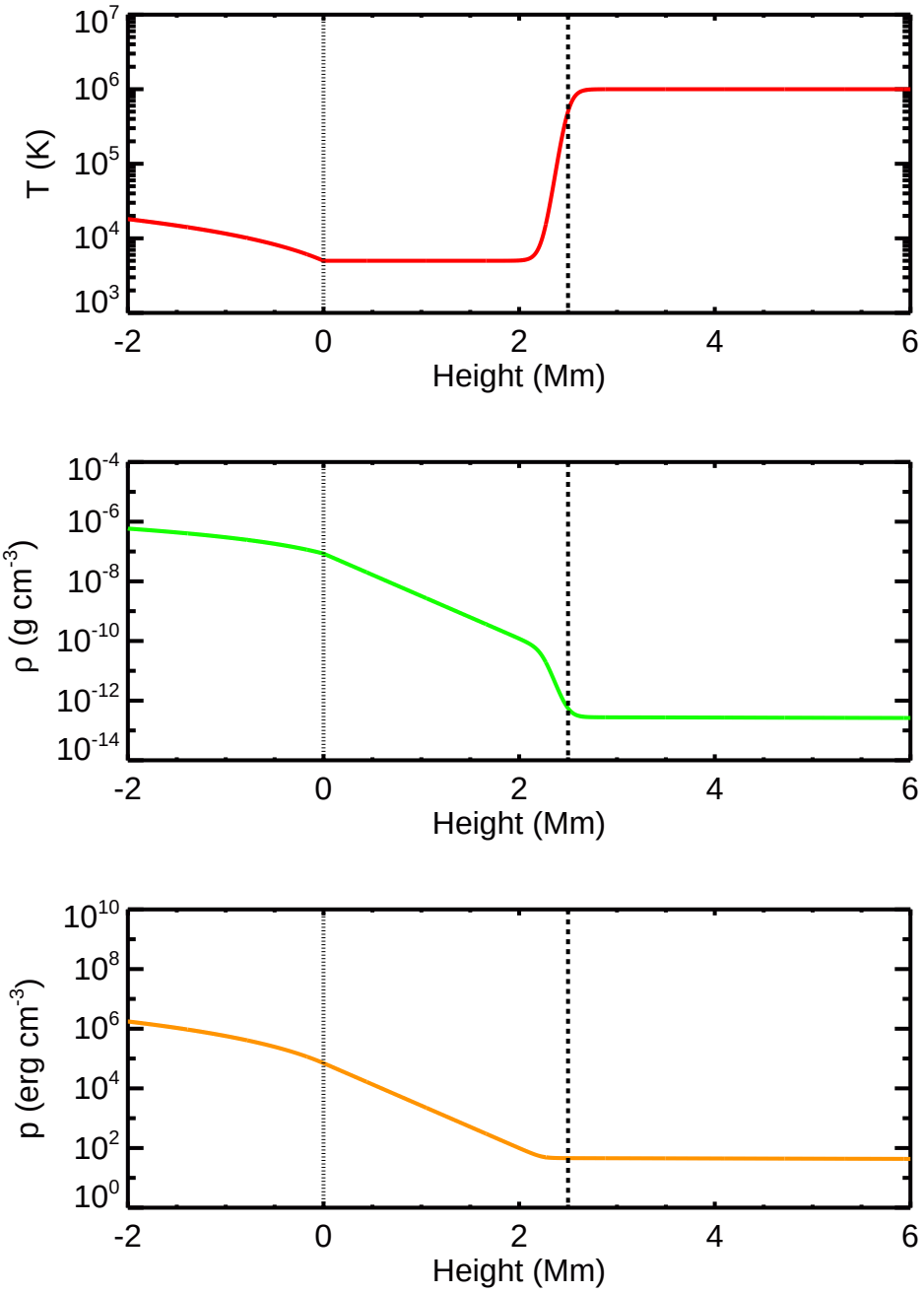

Figure 3.2: Initial temperature, density, and pressure distributions. The height of photosphere and transition region are shown in dotted and dashed line, respectively.

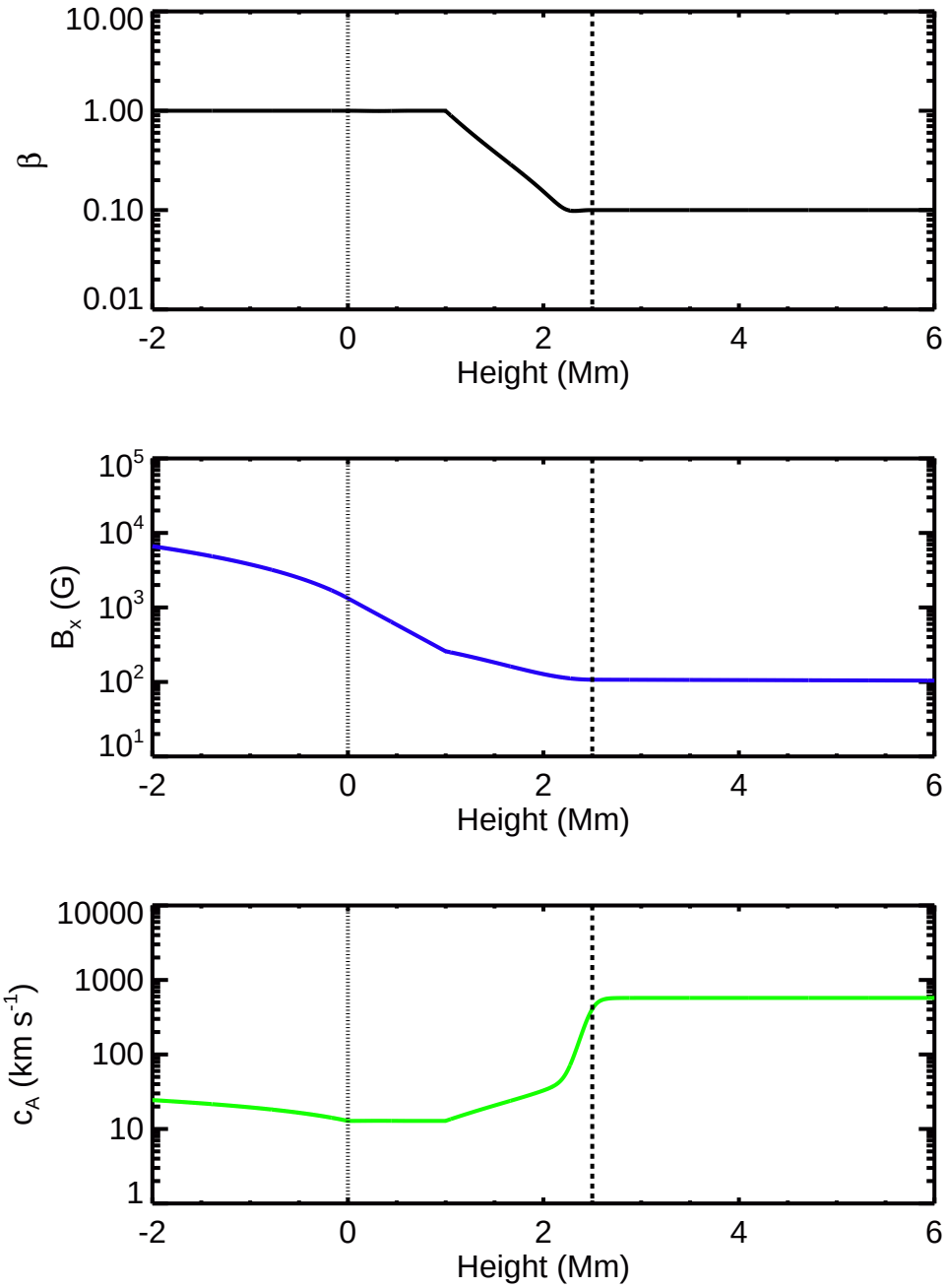

Figure 3.3: Distributions of plasma beta β, x component of the magnetic field B_x, and background Alfvén speed c_A in Case (I) with respect to height. The top, middle and bottom panels show the distributions of β, B_x and c_A, respectively.

3.2.3 Alfvén Wave Generator

We set a single sinusoidal Alfvénic pulse wave in initial state. Intial velocity amplitude of the pulse wave is given as the spatial function written as

$$v_y = v_{y0} \cdot f(x), \tag{3.14}$$

where v_{y0} is given as a parameter and $f(x)$ is determined as follow:

$$f(x) = \begin{cases} \sin\left(2\pi \frac{x-x_0}{\lambda_A}\right) & (x_0 \leq x \leq x_0 + \lambda_A/2) \\ 0 & (x < x_0,\ x_0 + \lambda_A/2 < x) \end{cases} \tag{3.15}$$

x_0 is the input height of the driver in the atmosphere. In our calculations, we investigate the propagation of Alfvénic pulse wave generated at the bottom of the photosphere, so x_0 is set as $x_0 = 0$ km in any cases. λ_A is a wavelength of sinusoidal Alfvén wave determined as follow:

$$\lambda_A = \frac{c_{A0}}{f}, \tag{3.16}$$

where c_{A0} is the Alfvén speed at $x = x_0$ and f is the wave frequency. The frequency is also given as a parameter. In order to drive the pulse wave propagating upward in the chromosphere, perturbation of transverse y component of the magnetic field is initially set as

$$B_y = -v_y \sqrt{4\pi\rho}, \tag{3.17}$$

which is based on Walén relation.

3.3 Numerical Set Up

The grid size is chosen to be $\Delta x = 0.81$ km in the range of $x \in [-L_0, L_0]$, where $L_0 = 10^4$ km, and it is larger as $\Delta x = 29.3$ km both below the height of $x = -L_0$ and above the height of $x = L_0$, since we focus on the wave propagation and dynamics in the

region around the chromosphere. We have rigid wall boundary conditions at both $z = -L$ and $z = L$ (where $L = 10^5$ km). The total number of grid points is 30720. The boundaries of numerical domain are set far enough from the photosphere and chromosphere in order to avoid to be affected by the reflected waves coming from the both boundaries. The numerical scheme we use in this thesis is the modified two-step Lax-Wendroff method (Rubin & Burstein, 1967) with artificial viscosity (Lapidus, 1967).

Chapter 4

Results

4.1 Wave Propagation

As explained in Chapter 3, the initial amplitude of Alfvénic pulse wave and frequency are given as parameters. At first, we present the results of Case (I) which has the plasma beta distribution assumed from Gary (2001). An upward propagating pulse is set at the bottom of the photosphere (upon $x = 0$ km). The initial amplitude is set as $v_{y0} = 1.0$ km s^{-1} in equation (3.14), which is approximately 10% of the background Alfvén speed (which is shown in Figure 3.3) at the launch height of $x = 0$ km.

Figure 4.1 shows the propagation of pulse with frequency at $f = 0.01$ Hz and Figure 4.2 shows the time variation of longitudinal velocity v_x and transverse velocity v_y as a gray scale. As the Alfvénic pulse propagates upward, x component of velocity appears from about $t = 60.0$ s. This longitudinal motion is the result of the nonlinear effect of Alfvén wave and becomes compressible wave mode. In the middle and upper chromosphere (where $1000 \leq x \leq 2500$ km), the propagation speed of Alfvénic pulse wave is approximately 25 km s^{-1} and that of the compressible wave is about 15 km s^{-1}. The compressible wave is slower than Alfvén wave because in the middle and upper chromosphere (above from the height of 1000 km), the plasma beta is smaller than unity. As waves propagate, the velocity amplitude of waves become larger due to the density strat-

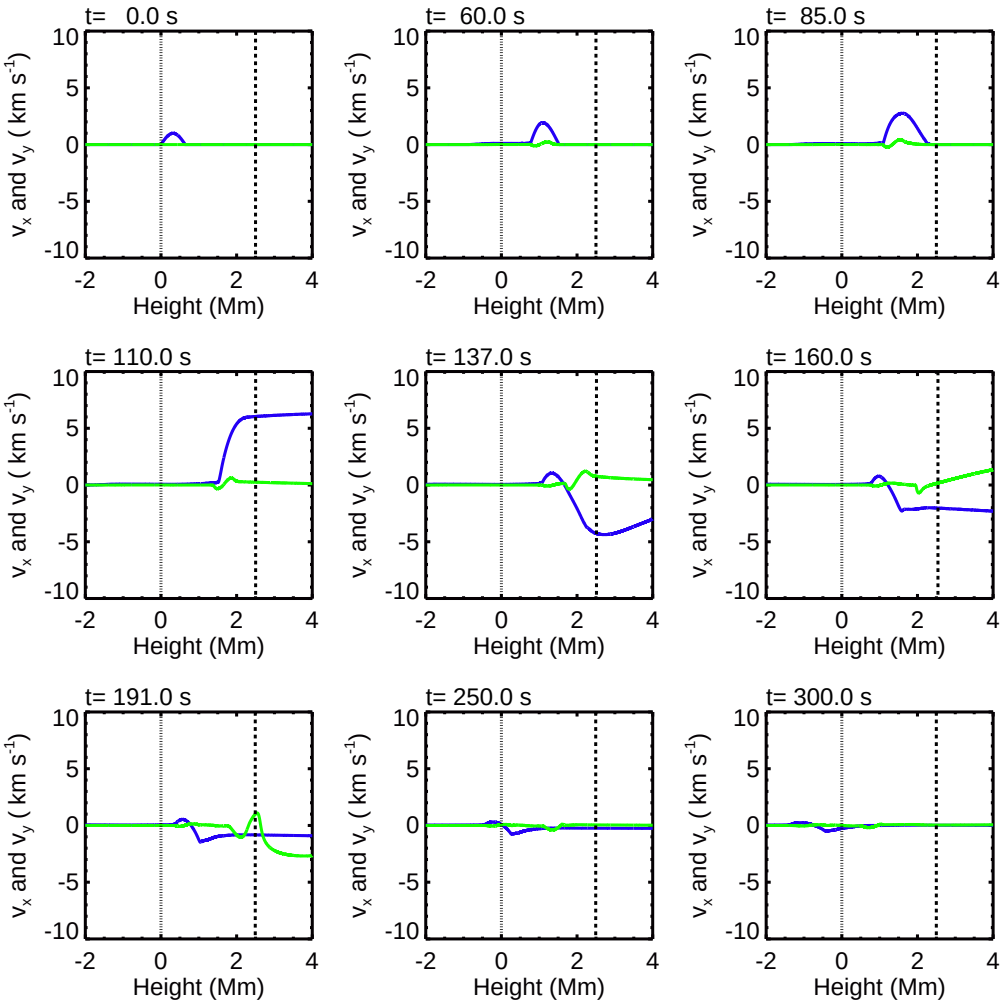

Figure 4.1: Evolution of the Alfvénic pulse. Reflection at the transition region and penetration of reflected pulse into the convection zone can be seen. Transverse velocity v_y is shown in blue line and longitudinal velocity v_x is shown in green line.

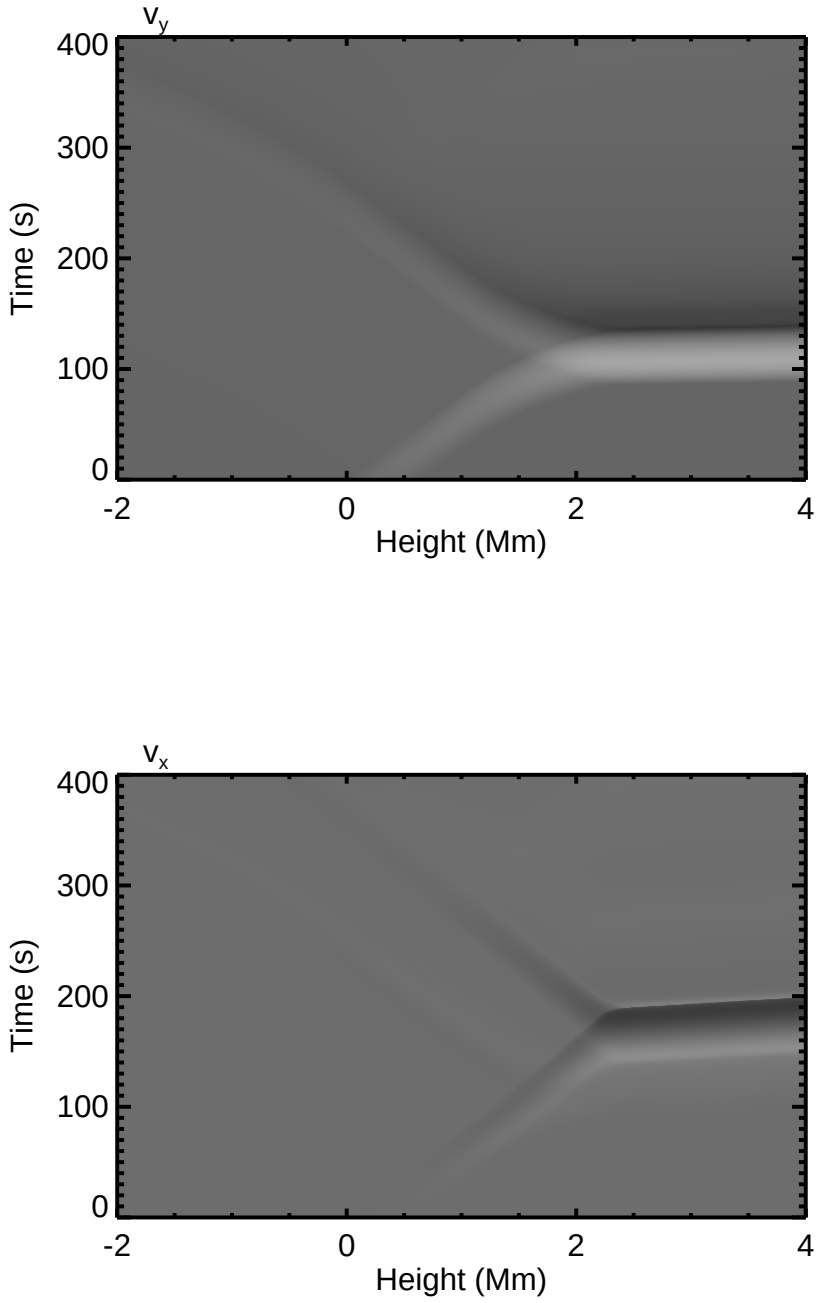

Figure 4.2: Time variation of transverse velocity v_y and longitudinal velocity v_x, which are shown as gray scale. The gray scale changes between the maximum and minimum of each variable.

ification. The velocity amplitude becomes about 5 km s^{-1} in the chromosphere. Before the compressible waves steepen and form shock waves, the Alfvénic pulse reaches the transition region height (at 2500 km which is shown in dashed lines in Figure 4.1) before $t = 85.0$ s. The reflection of the Alfvénic pulse wave occurs at $t = 110$ s. Most of the incident Alfvén waves are reflected and go back to the photosphere (at $t = 137$ s, $t = 160$ s, and $t = 270$ s). From $t = 250$ s to $t = 300$ s, most of the reflected Alfvén waves penetrate into the convection zone and it is difficult to see the reflection at the bottom of the photosphere.

4.2 Reflection Rate

In order to quantify the reflection of Alfvénic pulse wave, we calculate the temporal variation of the energy of Alfvén waves in the chromosphere. The energy density of Alfvén waves in the chromosphere is calculated by integrating from the height of photosphere $x = 0$ to that of the transition region $x = x_{\rm tr}$ as below:

$$E_{\rm AW} = \int_0^{x_{\rm tr}} \left(\frac{1}{2}\rho v_y^2 + \frac{B_y^2}{8\pi} \right) S \, dx \Big/ \int_0^{x_{\rm tr}} S \, dx. \tag{4.1}$$

Figure 4.3 shows the temporal variation of the energy density of Alfvén waves with initial velocity amplitude 1.0 km s^{-1} and relatively high frequency $f = 0.10$ Hz in the chromosphere in Case (I). The energy density is normalized by the Alfvén wave energy density in the initial state in the chromosphere $E_{\rm AW0}$. Time that the reflection of the incident Alfvénic pulse wave at the transition region occurs ($t = t_{\rm rf}$) is determined as the timing that the Alfvén wave energy density in the chromosphere decreases rapidly for the first time. The moment that the reflected wave pass through the photosphere into the convection zone ($t = t_{\rm pn}$) is determined as the timing that rapid decrease of the Alfvén wave energy density in the chromosphere occurs after the reflection at the transition region. In Figure 4.3, the vertical dashed line shows the time $t = t_{\rm rf}$ and dotted line shows the time

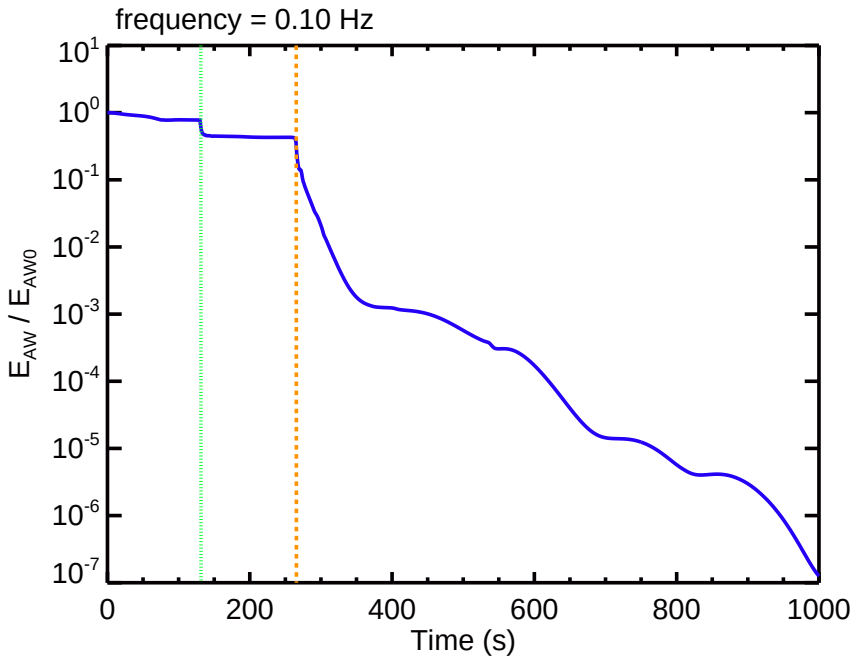

Figure 4.3: The temporal variation of the energy density of Alfvén waves with initial velocity amplitude 1.0 km s^{-1} and frequency $f = 0.10$ Hz in the chromosphere in Case (I) calculated from equation (4.1). The energy density is normalized by the initial Alfvén wave energy density. The green dotted line shows the time of the reflection of incident Alfvénic pulse wave at the transition region (when $t = t_{\rm rf}$) and orange dashed line shows that of the penetration of reflected wave into the convection zone (when $t = t_{\rm pn}$).

$t = t_{\rm pn}$. After the reflection of incident Alfvénic pulse wave at the transition region occurs, some of the energy of Alfvén waves are trapped in the chromosphere (in the period of $t_{\rm rf} \leq t \leq t_{\rm pn}$). After $t = t_{\rm pn}$, the Alfvén wave energy density in the chromosphere rapidly decreases to 10^{-7} times the initial Alfvén wave energy density. This indicates that most of reflected waves penetrate into the convection zone through the bottom of the photosphere without reflection.

Reflection rate at the transition region is calculated as the ratio of the energy density of Alfvén waves in the chromosphere when one wave period before the reflection at the transition region occurs ($t = t_{\rm rf}$) to that when one wave period after $t = t_{\rm rf}$. The reflection rates are calculated in the cases of wave frequencies at $f = 0.01$, 0.02, 0.04, 0.06, 0.08, and 0.10 Hz. The variation of reflection rate with respect to the wave frequency is shown in Figure 4.4. We can see the reflection rates tend to decrease from about 0.7 at $f = 0.01$

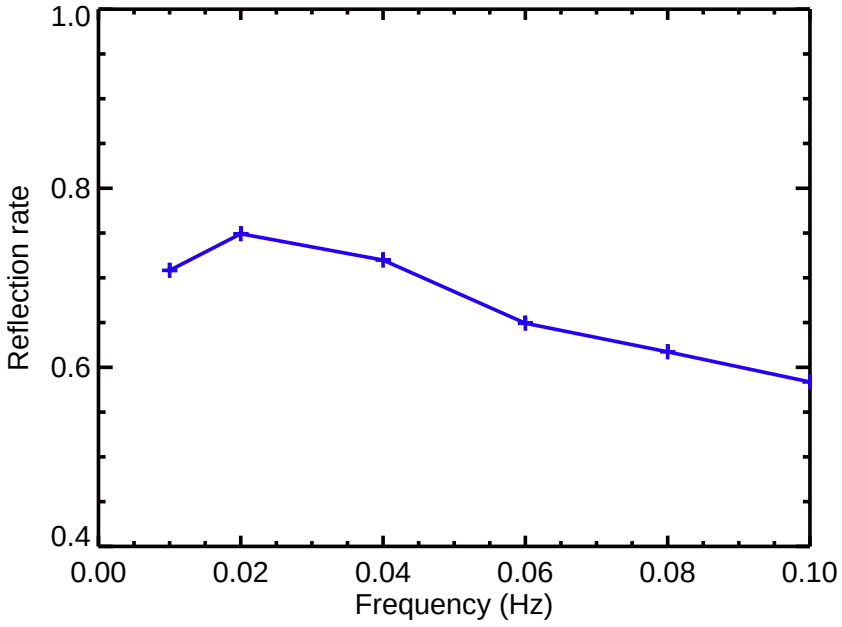

Figure 4.4: Variation of the reflection rate of the incident Alfvénic pulse waves at the transition region in Case (I) with respect to wave frequency. The initial velocity amplitude of the incident pulse wave is set to be 1.0 km s^{-1}.

Hz to about 0.6 at $f = 0.10$ Hz. The higher wave frequency means that wave length

becomes shorter compared to the background Alfvénic scale height and the wave easily penetrate through the boundary. This indicates that more Alfvén waves are reflected at the transition region at lower frequency, which can be seen from the result shown in Figure 4.4.

In Case (I), most of reflected Alfvén waves penetrate into the convection zone through the bottom of the photosphere. Even though relatively lower frequency ($f = 0.01$ Hz) with larger wavelength is set, the reflection at the bottom of the photosphere is weak. This implies that the typical atmosphere assumed from the plasma beta model in Gary (2001) is difficult to trap the Alfvén waves in the chromosphere.

4.3 Comparison in Different Magnetic Field Structures

In Case (I), it is found that more than 50 % of the incident Alfvén waves are reflected at the transition region and most of the reflected waves penetrate into the convection zone. Since we are interested in the condition which more Alfvén waves are trapped in the chromosphere, in addition to Case (I), two different structures are considered. One is the condition which has the similar plasma beta distribution to that is used in Kudoh & Shibata (1999) and Matsumoto & Shibata (2010). This profile is in the range of plasma beta model given in Gary (2001). In the photosphere and low chromosphere (where $0 \leq x \leq 1000$ km), the plasma beta is larger than unity, and becomes smaller than unity above the height of 1000 km. In the convection zone (where $x \leq 0$ km), the plasma beta is assumed to be unity and constant. We henceforth call this as Case (Ⅱ). The other is the distribution which has the constant and unit plasma beta in a whole region. This case is referred to as Case (Ⅲ). Comparison between these plasma beta distributions in three cases are shown in Figure 4.5. The distributions of x component of the background magnetic field which is calculated from equation (3.12) and the background Alfvén speed (which is calculated as $c_A = B_x/\sqrt{4\pi\rho}$) are shown in Figure 4.6 and Figure 4.7, respectively. In Case (Ⅱ), there are steep decreases of magnetic field strength at the bottom of the photosphere, and

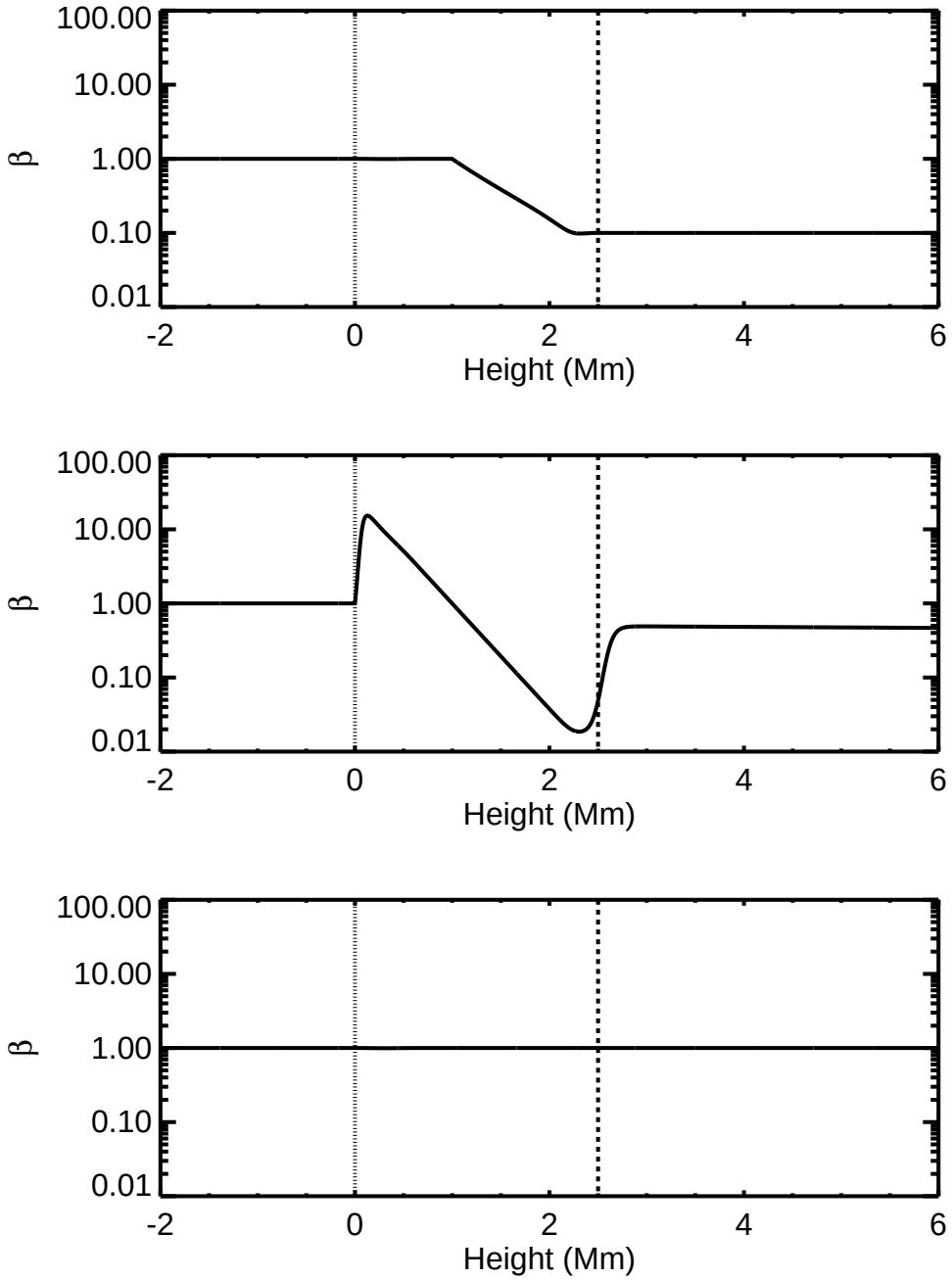

Figure 4.5: Comparison of the distributions of plasma beta with respect to height. The top, middle and bottom panels show the distributions in Case (I), (II) and (III), respectively.

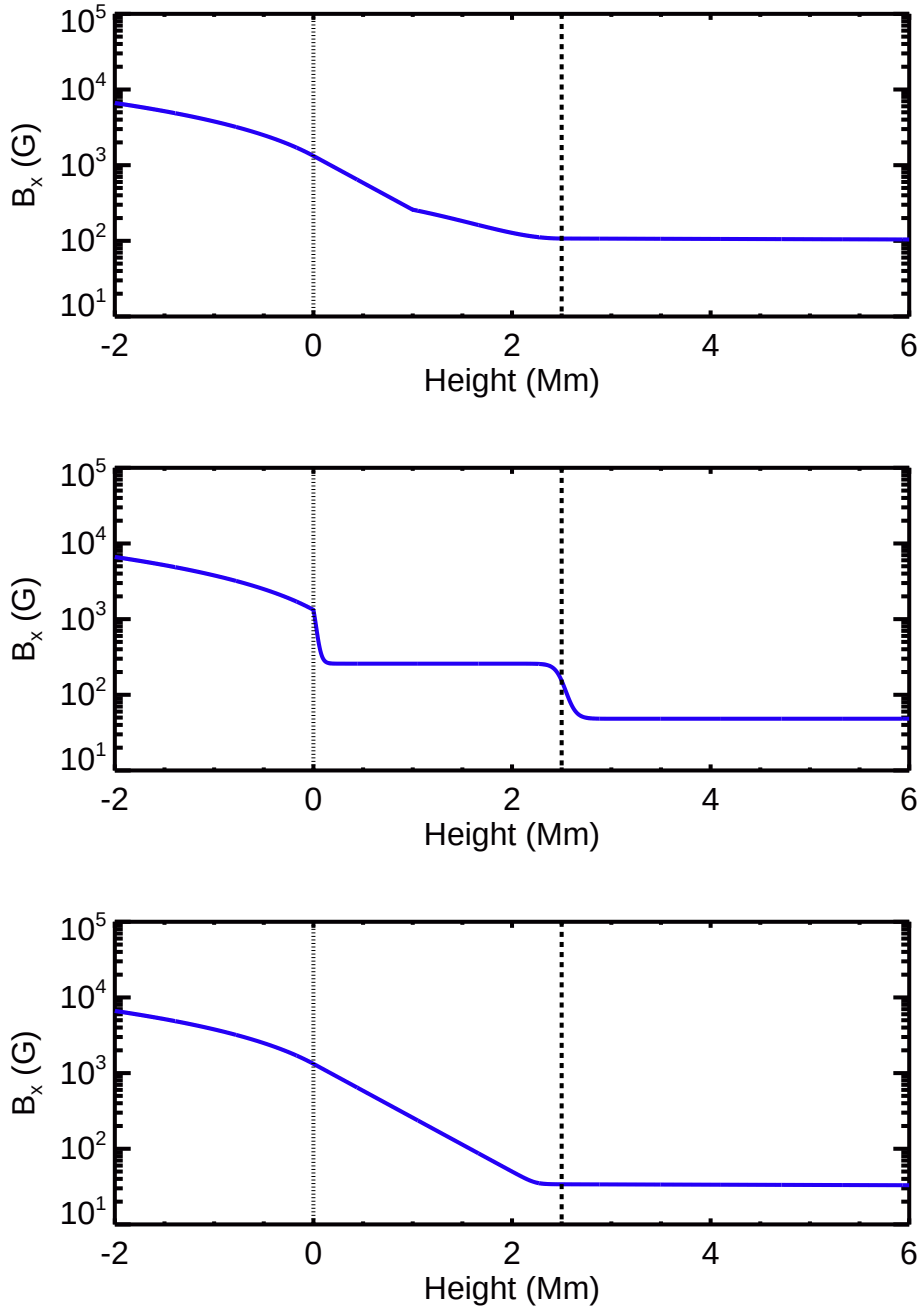

Figure 4.6: Comparison of distributions of x component of the magnetic field. The top, middle and bottom panels show the distributions in Case (I), (II) and (III), respectively.

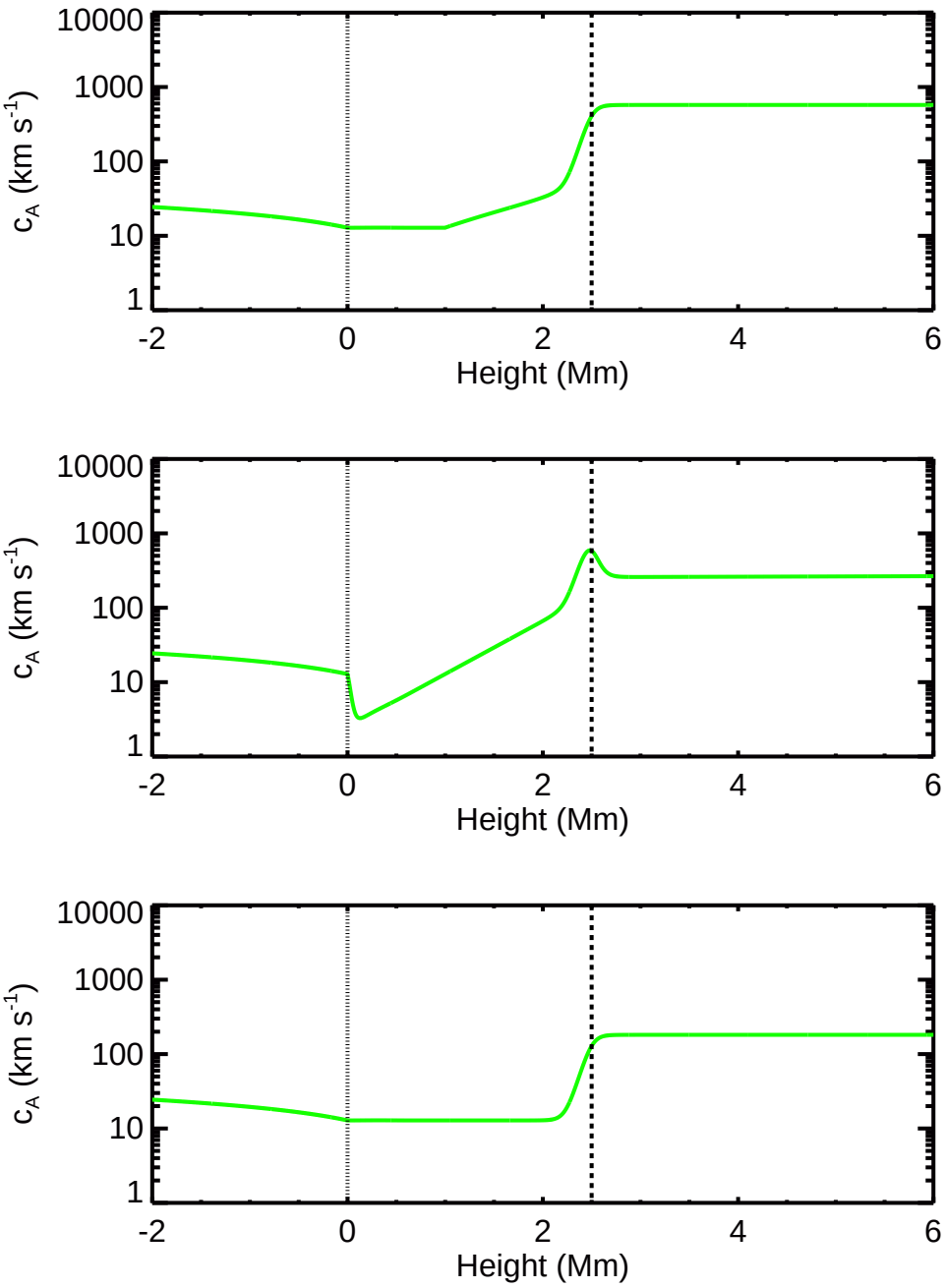

Figure 4.7: Comparison of distributions of the background Alfvén speed. The top, middle and bottom panels show the distributions in Case (I), (II) and (III), respectively.

at the transition region. If the background Alfvénic scale height is much smaller than the wavelength of propagating Alfvén waves, those waves are reflected more at the boundary. Case (Ⅱ) is thought to correspond to the condition that more Alfvén waves may be trapped in the chromosphere. In order to investigate the effect of steep variation of the magnetic field strength, we consider the Case (Ⅲ) for comparison. The Alfvén speed in the middle and upper chromosphere, and corona in Case (Ⅲ) is smaller than that in Case (I) and Case (Ⅱ).

The comparison of the energy density of Alfvén waves with initial amplitude of 1.0 km s^{-1} and frequency of 0.10 Hz in the chromosphere is shown in Figure 4.8. We can

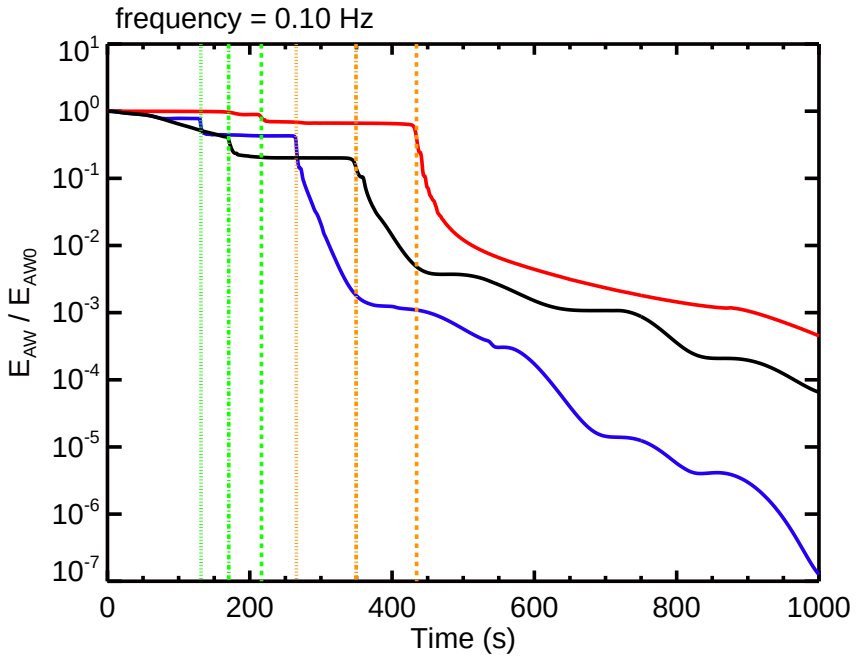

Figure 4.8: Comparison of the energy density of Alfvén waves with initial velocity amplitude 1.0 km s^{-1} and frequency 0.10 Hz in the chromosphere. The energy density is calculated from equation (4.1) and normalized by the initial Alfvén wave energy density. The blue, red, and black solid lines show the temporal variation of the energy density in Case (I), Case (Ⅱ), and Case (Ⅲ), respectively. The green vertical lines show the time that incident Alfvénic pulse wave is reflected at the transition region (when $t = t_{\rm rf}$) and orange ones show the time that reflected waves penetrate into the convection zone ($t = t_{\rm pn}$). In these vertical lines, the dotted, dashed, and dashed-dotted lines indicate the time in Case (I), Case (Ⅱ), and Case (Ⅲ), respectively.

see, after the reflection of the incident Alfvénic pulse wave at the transition region, more

Alfvén wave energy remains in the chromosphere in Case (Ⅱ) than in Case (I), and the more energy is lost in Case (Ⅲ) than the other cases. In any cases, the Alfvén wave energy in the chromosphere decreases rapidly after the penetration of Alfvén waves into the convection zone.

We calculate the variation of reflection rates of Alfvénic pulse waves at the transition region with respect to frequency in Case (I), (Ⅱ), (Ⅲ). Figure 4.9 shows the comparison of reflection rates between three cases. The reflection rates are larger in Case (Ⅱ) than

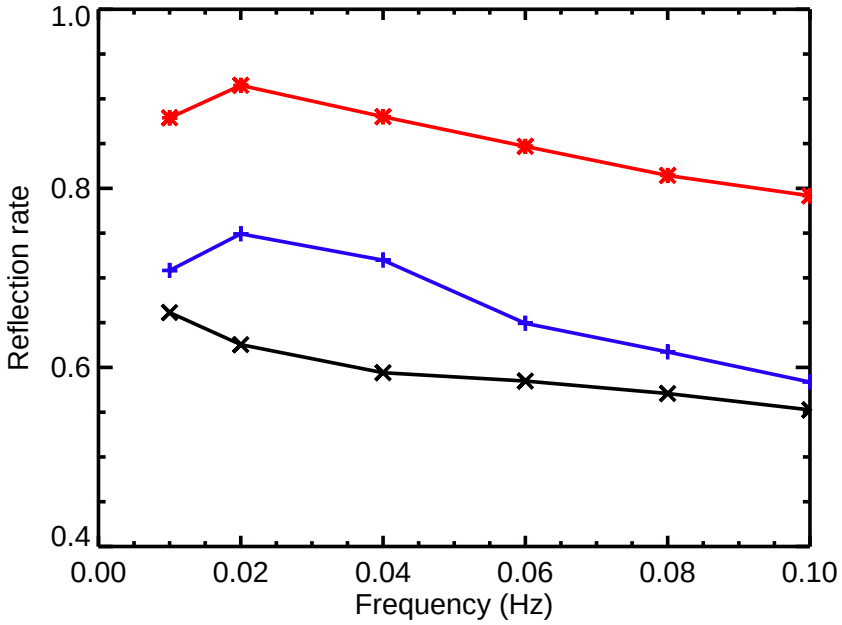

Figure 4.9: Comparison of the reflection rates of Alfvénic pulse waves with initial velocity amplitude 1.0 km s^{-1} at the transition region in Case (I), Case (Ⅱ) and Case (Ⅲ). The variation of reflection rates with respect to wave frequency are shown. The blue, red and black lines show the variation of reflection rates in Case (I), Case (Ⅱ) and Case (Ⅲ), respectively.

Case (I) at any frequencies, and smaller in Case (Ⅲ). The reason why the reflection rate increases (or decreases) and more (or less) Alfvén waves trapped in the chromosphere in Case (Ⅱ) (or Case (Ⅲ)) than Case (I) can be considered from the distributions of background Alfvén speed in the chromosphere shown in Figure 4.7. In the studied cases, the background Alfvénic scale height at the transition region is almost equal. In Case (Ⅱ), the

plasma beta is set to be larger than unity in the photosphere and low chromosphere (where $0 \leq x \leq 1000$ km), and smaller than that in Case (I) in the middle and upper chromosphere (where $1000 \leq x \leq 2500$ km). This means that the background Alfvén speed in Case (Ⅱ) becomes smaller than Case (I) in the photosphere and low chromosphere, and larger in the middle and upper chromosphere. In such a situation like Case (Ⅱ), as the incident Alfvénic pulse wave propagates upward in the chromosphere, the wavelength becomes much larger before the pulse reaches to the transition region height. This wider wavelength created in Case (Ⅱ) is thought to cause more reflection at the transition region than Case (I). On the other hand, in Case (Ⅲ), the background Alfvén speed in the middle and upper chromosphere is set to be smaller than Case (I) and Case (Ⅱ). The incident Alfvénic pulse wave propagates upward in the chromosphere with almost constant wavelength and the reflection rates become smaller than the other cases. From the comparison, it is concluded that the condition where the background Alfvén speed increases from the photosphere to the upper chromosphere cause more reflection at the transition region.

In any cases, most of reflected waves propagate downward to the photosphere and penetrate through the bottom of the photosphere into the convection zone. Even in Case (Ⅱ), which has steep variation of the magnetic field strength and small Alfvénic scale height at the bottom of the photosphere, Alfvén wave energy density in the chromosphere decreases after the reflected waves reach to the convection zone. This result indicates that it is difficult to trap the Alfvén waves inside the chromosphere because most of the downward propagating waves in the chromosphere penetrate into the convection zone.

4.4 Mode Conversion

We calculate how much Alfvén wave is energy converted into compressible wave energy. The energy density of compressible waves in the chromosphere is calculated as below:

$$E_{\mathrm{CW}} = \int_0^{x_{\mathrm{tr}}} \frac{1}{2}\rho v_x^2 S \, dx \Big/ \int_0^{x_{\mathrm{tr}}} S \, dx. \tag{4.2}$$

Figure 4.10 shows temporal variation of the Alfvén wave energy density and compressible wave energy density in the chromosphere in Case (I). As the Alfvén wave energy in the chromosphere decreases, the compressible wave energy increases to about 0.07 times the initial Alfvén wave energy. The compressible wave energy decreases gradually with time after it reaches to the maximum value.

Figure 4.11 shows the variation of the maximum value of the compressible wave energy in the chromosphere with respect to wave frequency f. The energy density of generated compressible waves in the chromosphere increases from 0.01 at $f = 0.01$ Hz to 0.07 at $f = 0.10$ Hz. We can see more compressible wave energy is generated in the case with higher wave frequency. This result is expected from that the nonlinearity of the wave becomes larger at higher frequency. The more compressible wave modes are generated in the case with higher frequency than lower frequency due to the stronger nonlinear mode conversion effect.

We compare the compressible wave energy in three cases, which have different magnetic field structures shown in section 4.3. Comparison of the maximum value of the compressible wave energy in the chromosphere at each frequency is shown in Figure 4.12. We can that see more compressible wave energy is generated in the order of Case (Ⅲ), Case (I), Case (Ⅱ) at any frequencies. As explained in previous section, in Case (Ⅱ), the larger background Alfvén speed in the middle and upper chromosphere and the smaller Alfvén speed in the photosphere and the low chromosphere make the wavelength of the incident Alfvénic pulse wave larger. This reduces the nonlinearity of the pulse wave in Case (Ⅱ) and less compressible waves are generated in the chromosphere. On the other hand, Alfvénic pulse wave with smaller wavelength in Case (Ⅲ) has larger nonlinearity and generate more compressible waves in the chromosphere.

We estimate the possible heating rates from the fraction of compressible waves generated from the single Alfvénic pulse wave. In the studied cases, the generated compressible wave energy is about 10^{-3}–10^{-1} times the initial Alfvén wave energy. If we assume that the input energy flux is calculated as $F_{\mathrm{AW0}} = \rho_0 v_0^2 c_{A0}$, where ρ_0 is the total mass density

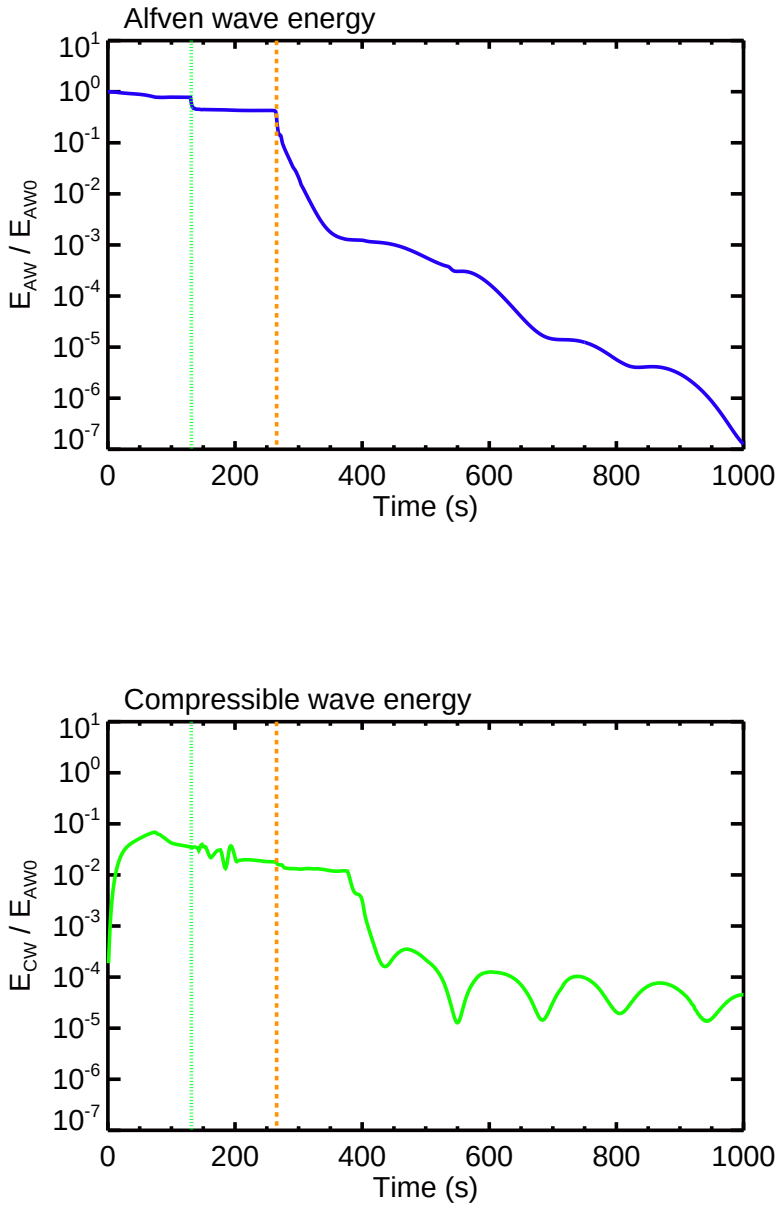

Figure 4.10: The temporal variation of wave energy density in the chromosphere in Case (I). The initial velocity amplitude is set to be 1.0 km s^{-1} and the frequency is set as $f = 0.10$ Hz. The top panel shows the energy density of Alfvén waves and the bottom panel shows that of compressible waves. The vertical green dotted line shows the time when $t = t_{\rm rf}$ and the orange dashed line shows $t = t_{\rm pn}$

.

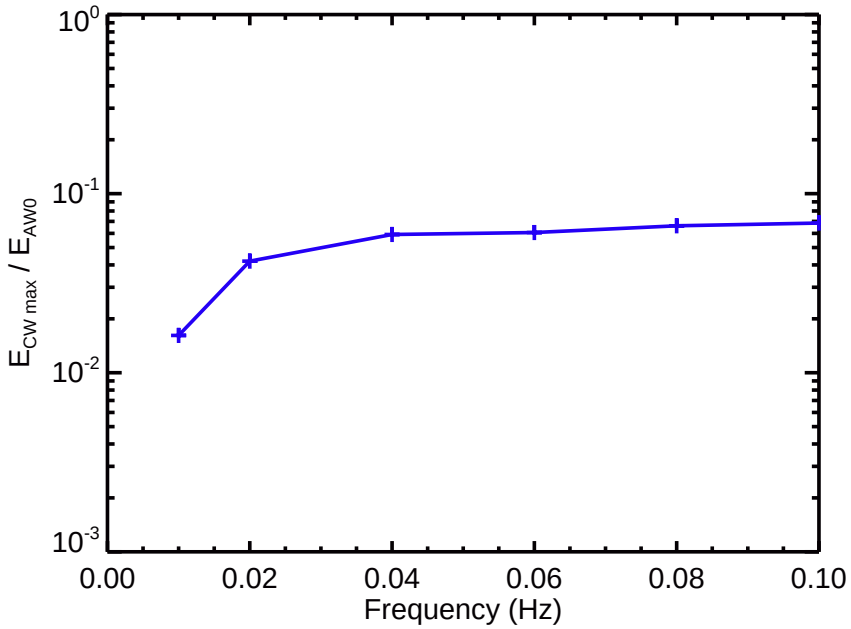

Figure 4.11: Variation of the maximum value of the compressible wave energy density in the chromosphere in Case (I) with respect to wave frequency. The initial velocity amplitude is set to be 1.0 km s^{-1}.

at the bottom of the photosphere, v_0 the initial velocity amplitude at the photosphere, c_{A0} the background Alfvén speed at the bottom of the photosphere, the compressible wave energy generated in the chromosphere is estimated as $F_{\rm CW} = 10^{-3}$–$10^{-1} F_{\rm AW0}$. If we give the values $\rho_0 = 10^{-7}$ g cm^{-3}, $v_0 = 1.0$ km s^{-1}, and $c_{A0} = 10$ km s^{-1}, the input Alfvén energy flux is calculated as $F_{\rm AW0} = 10^9$ erg cm^{-2} s^{-1} and the generated compressible wave energy is estimated as $F_{\rm CW} = 10^6$–10^8 erg cm^{-2} s^{-1}. If this compressible wave energy is dissipated by forming shock waves and converted into thermal energy in the chromosphere, the generated thermal energy may be comparable to the total required energy flux to heat the chromosphere, which is 4×10^6 erg cm^{-2} s^{-1} estimated by Withbroe & Noyes (1977) (shown in Table 1.1). We confirm that shock waves are formed in the chromosphere in our calculations with frequencies of 0.02–0.10 Hz. From the results, the compressible waves generated from the single Alfvénic pulse wave in the all studied cases have possibility to heat the chromosphere.

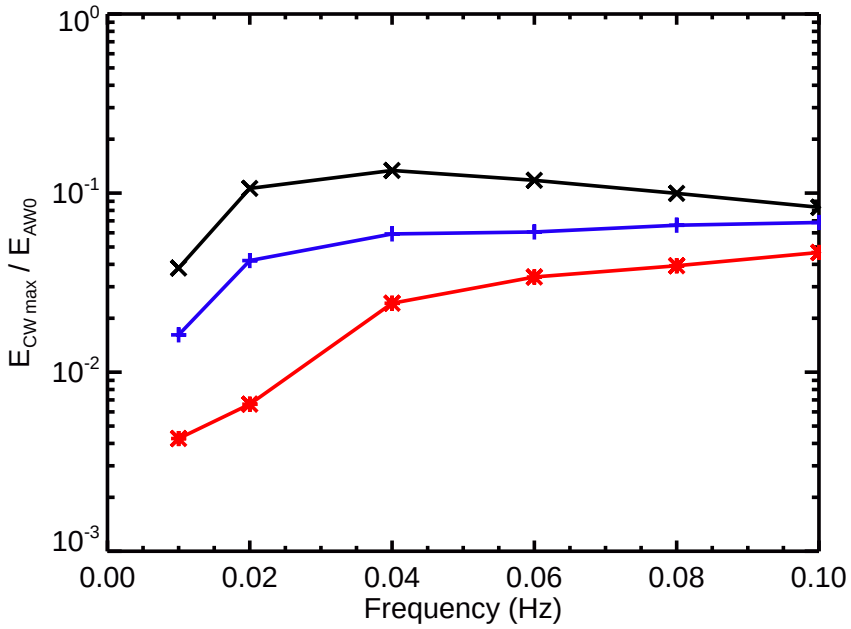

Figure 4.12: Comparison of the maximum value of the compressible wave energy density in the chromosphere in Case (I), (II), (III). The initial velocity amplitude is set to be 1.0 km s^{-1}. The variation of the maximum value of the compressible wave energy with respect to wave frequency is shown. The blue, red and black lines show the variation of the compressible wave energy in Case (I), (II) and (III), respectively.

We perform the calculations with smaller initial velocity amplitude which is set as $v_{y0} = 0.1$ km s^{-1} in equation (3.14), and investigate the contribution for the chromospheric heating. We calculate the compressible wave energy density generated from single Alfvénic pulse wave in the chromosphere for the case with smaller initial velocity amplitude. Comparison of the generated compressible wave energy between the case with initial velocity amplitude 1.0 km s^{-1} and 0.1 km s^{-1} in Case (I) is shown in Figure 4.13. Alfvénic pulse wave with smaller velocity amplitude (0.1 km s^{-1}) has weaker non-

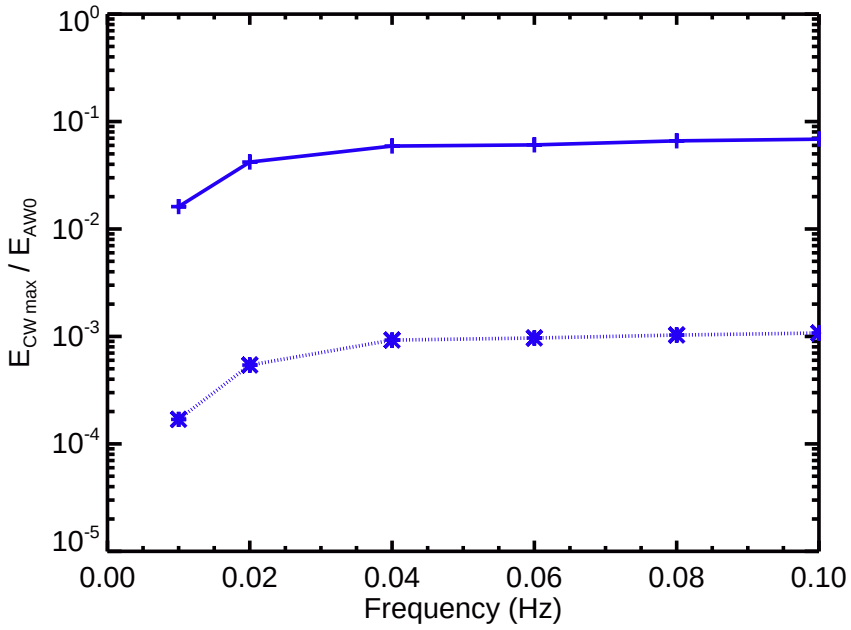

Figure 4.13: Comparison of the maximum value of the compressible wave energy density in the chromosphere between the case with larger initial velocity amplitude 1.0 km s^{-1} and smaller initial velocity amplitude 0.1 km s^{-1}. The variation of the maximum value of the compressible wave energy with respect to wave frequency is shown. The blue solid lines show the variation of the compressible wave energy in the case with initial velocity amplitude 1.0 km s^{-1}. The blue dotted line shows the result in the case with initial velocity amplitude 0.1 km s^{-1}.

linearity and less compressible wave modes are generated. The generated compressible wave energy is about 10^{-4}–10^{-3} times the initial Alfvén wave energy. This compressible wave energy is 10^{2} times less than the results with initial velocity amplitude 1.0 km s^{-1}. Since the initial Alfvén energy flux is calculated as $F_{\rm AW0} = \rho_0 v_0^2 c_{A0} = 10^7$ erg cm^{-2} s^{-1},

where $\rho_0 = 10^{-7}$ g cm^{-3}, $v_0 = 0.1$ km s^{-1}, and $c_{A0} = 10$ km s^{-1}, the generated compressible wave energy is estimated as $F_{\rm CW} = 10^3$–10^4 erg cm^{-2} s^{-1}. This energy is much less than required value in Withbroe & Noyes (1977). For the dissipation of Alfvén waves with smaller velocity amplitude (0.1 km s^{-1}), the nonlinear mode conversion occurs less than those with larger velocity amplitude (1.0 km s^{-1}) and other dissipation mechanisms (such as magnetic diffusion) may become effective.

Chapter 5

Discussion

We presented the analytic estimates of the effect of magnetic diffusion in the chromosphere to the nonlinear propagation of Alfvén waves in Chapter 2, and the results of 1.5D numerical simulations in Chapter 4.

5.1 The Effect of Magnetic Diffusion

In the analytic estimates, we calculated magnetic diffusivity along an open magnetic flux tube. The effect of presence of neutrals has been taken into account for calculating the magnetic diffusivity. The ambipolar diffusion, which is caused by the collision between charged particles and neutrals, enhances the magnetic diffusion in the chromosphere. The damping of Alfvén waves by magnetic diffusion in the partially ionized chromosphere has been investigated in various studies.

Goodman (2011) estimated the conditions for linear, non-plane Alfvén waves driven in the photosphere to heat the chromosphere. In his conclusion, waves with frequencies 0.1–1.0 Hz for background magnetic field strengths $B \geq 700$ G and magnetic field perturbation amplitude ~ 0.01–$0.1B$ can give sufficient heating rate in the chromosphere. The amplitude is almost similar to the values which we analyzed here, however, his frequencies are relatively high and the magnetic field strength is assumed to be strong and uniform in vertical direction. This higher frequency and stronger magnetic field may cause strong

damping of Alfvén waves in the chromosphere because the magnetic diffusivity coefficient of ambipolar diffusion term $\tilde{\eta}_A \propto |B|^2$ and the damping length $L_d \propto \eta^{-1} f^{-2}$. In our analysis, the wave frequency is set as $f = 10^{-3}$–10^{-1} Hz and the magnetic field strength decreases with height from about 1500 G in the photosphere to 50 G in the corona. In this condition, the damping length is calculated much longer than the height of transition region above the photosphere, so the magnetic diffusion may be effective if the much Alfvén waves are reflected at the boundaries of the chromosphere and trapped inside the layer.

In Leake et al. (2005) and Kazeminezhad & Goodman (2006), one-dimensional numerical MHD models of damping of Alfvén waves were presented. However, those models include only the middle and upper chromosphere. It is important to investigate the propagation of Alfvén waves from the photosphere to the corona for the chromospheric heating because Goodman (2011) proposed that the energy flux going into the chromosphere is regulated by the ohmic diffusion in the photosphere, and moreover our results of numerical calculations suggested the importance of the reflection at the transition region and the penetration at the bottom of the photosphere.

5.2 Nonlinear Propagation of Alfvén Waves

We investigated the nonlinear propagation of Alfvénic pulse wave along a vertical and open magnetic flux tube. The main difference from the previous studies is treatment at the bottom boundary of the photosphere. Matsumoto & Shibata (2010) proposed the model that the solar atmosphere is strongly heated by the Alfvén wave resonance between the photosphere and transition region. They assumed the convective motions are dominant and the magnetic fields are easily bent below the photosphere. In such a condition, the bottom of the photosphere is treated as the rigid boundary and becomes a node of the resonance. In our numerical calculation, the magnetic flux tube is assumed to be connecting into the deeper layer of the convection zone and the condition in the convection zone is

based on the assumption of adiabatic stratification. Our results showed that, even though there is steep variation of background Alfvén speed at the bottom of the photosphere, most of waves penetrate into the convection zone through the photosphere. We suggest that, for the chromospheric heating, not only the energy flux penetrates into the corona but also into the convection zone should be considered.

In Matsumoto & Shibata (2010), strong Alfvén wave resonance has been confirmed to occur with frequencies at $1, 3,$ and 5 mHz. We should investigate the effect of waves with such lower frequencies by setting the continuous wave driver at the bottom of the photosphere. In addition to that, Matsumoto & Shibata (2010) includes the effect of radiative cooling. That effect may also affect the calculation of heating rate in the chromosphere.

James et al. (2003) have calculated the reflection rate of the Alfvénic pulse at the transition region by performing 1.5D MHD numerical simulation. They set wave frequencies ~ 0.1–0.5 Hz which are higher than those in our simulation model. In their model, the effect of magnetic diffusion including the ion-neutral collision is taken into account, and the atmospheric condition is given from VAL-C model. For the background magnetic field, the potential field model is taken and the strength decreases from 1600 G at the photosphere to 10–40 G in the corona. The reflection rate of wave frequency at 0.10 Hz is calculated as ~ 0.95 in their results. In our results, the reflection rate of wave frequency at $f = 0.10$ Hz in Case (I) which has the plasma beta distribution assumed from the model in Gary (2001) is about 0.6 and relatively smaller than the result in James et al. (2003). We calculated the reflection rate in different magnetic field structures and confirmed that the more reflection is occurred if the background Alfvén speed changes with height from the photosphere to the upper chromosphere. The larger reflection rate is calculated in Case (II). The reflection rate of wave frequency at 0.10 Hz becomes about 0.8 and almost comparable to the value in James et al. (2003).

5.3 Observational Constraints

In our calculations, the velocity amplitude of Alfvén wave becomes larger as wave propagates upward in the chromosphere. The maximum value of velocity amplitude in the chromosphere is about 5–15 km s^{-1} if the initial velocity amplitude is set to be 1.0 km s^{-1}. The mean amplitude of observed waves propagating along the solar spicules are 7.4 ± 3.7 km s^{-1} in Okamoto & De Pontieu (2011). In detail, De Pontieu et al. (2012) characterized spicules by three different types of motion: field-aligned flows of order 50–100 km s^{-1}, swaying motions of order 15–20 km s^{-1}, and torsional motions of order 25–30 km s^{-1}. These values of amplitudes cannot be seen in our numerical calculation results. Since we have investigated a single Alfvénic pulse wave, which does not have enough power to push up the transition region to the observed height of spicules $\sim 10^4$ km. In order to compare the calculated wave amplitude with observational values, the formation of spicules may be the future work.

Chapter 6

Summary and Future Prospects

We have performed analytic calculations and 1.5D MHD numerical simulations for the chromospheric heating. Alfvén waves generated by the photospheric convection motion is thought to carry enough energy to heat the solar atmosphere, for especially the low-plasma-beta region such as the middle and upper chromosphere, and corona. As the dissipation mechanism of Alfvén waves, two possibilities are considered. One is the damping by magnetic diffusion and the other is the nonlinear mode conversion and associated shock dissipation.

In the chromosphere, the ionization degree is low ($\sim 10^{-4}$ at minimum in VAL-C model given in Vernazza et al., 1981) and the plasma gas is partially ionized. The ambipolar diffusion is caused by collision between charged particles and neutrals. We calculated analytically the damping length of Alfvén waves in the chromosphere by magnetic diffusion which takes the ambipolar diffusion into account. The damping length has been calculated as much longer than the thickness of the chromosphere ($> 10^3$ km) for the magnetic field strength which decreases from 1500 G at the photosphere to 50 G in the corona. For the chromospheric heating, it is important to estimate how much Alfvén waves are reflected at bottom and top boundaries of the chromosphere (which are corresponding to the photosphere and transition region, respectively) and trapped inside the layer.

We have investigated the nonlinear propagation of Alfvénic pulse waves along a vertically open magnetic flux tube from the convection zone to the corona by performing 1.5D MHD numerical calculations. The reflection rates at the transition region have been calculated in different magnetic field structures. In typical case, about 60–70 % of the incident Alfvén waves with initial velocity amplitude 1.0 km s^{-1} and frequency at 0.01–0.10 Hz are reflected at the transition region. It is shown that the reflection rate is strongly dependent on the background Alfvén speed in the chromosphere. If the background Alfvén speed increases from the photosphere to the transition region, the wavelength of Alfvén wave becomes larger and more reflections at the transition region occur. Moreover, the larger Alfvén wavelength reduces the nonlinearity of the wave and less compressible wave modes are generated by mode conversion from the Alfvén waves. It is also indicated that most of the waves penetrate into the convection zone without being reflected at the bottom of the photosphere. It implies that, for estimating the heating rate due to the dissipation of Alfvén waves in the chromosphere, we should consider the energy flux going into not only the corona from the top but also the convection zone from the bottom of the chromosphere. The compressible wave energy generated from the single Alfvénic pulse wave with initial velocity amplitude 1.0 km s^{-1} is estimated as about 10^6–10^8 erg cm^{-2} s^{-1}. If the compressible waves is assumed to dissipate in the chromosphere by forming shock waves, this energy becomes comparable to the required total energy to heat the chromosphere. On the other hand, Alfvén waves with smaller initial velocity amplitude 0.1 km s^{-1} produce much less compressible waves, which are not enough to heat the chromosphere. For such Alfvén waves with smaller velocity amplitude, the dissipation mechanisms such as magnetic diffusion may be effective. Theses are summarized in Figure 6.1.

In this thesis, we assumed ideal MHD in numerical simulations. Taking the non-adiabatic effects, such as heating due to the magnetic diffusion or radiative cooling into account might be the future work. We will confirm the effect of magnetic diffusion in partially ionized gas from numerical simulations. The radiative cooling process might affect the dissipation of waves in the chromosphere. For calculating such non-adiabatic

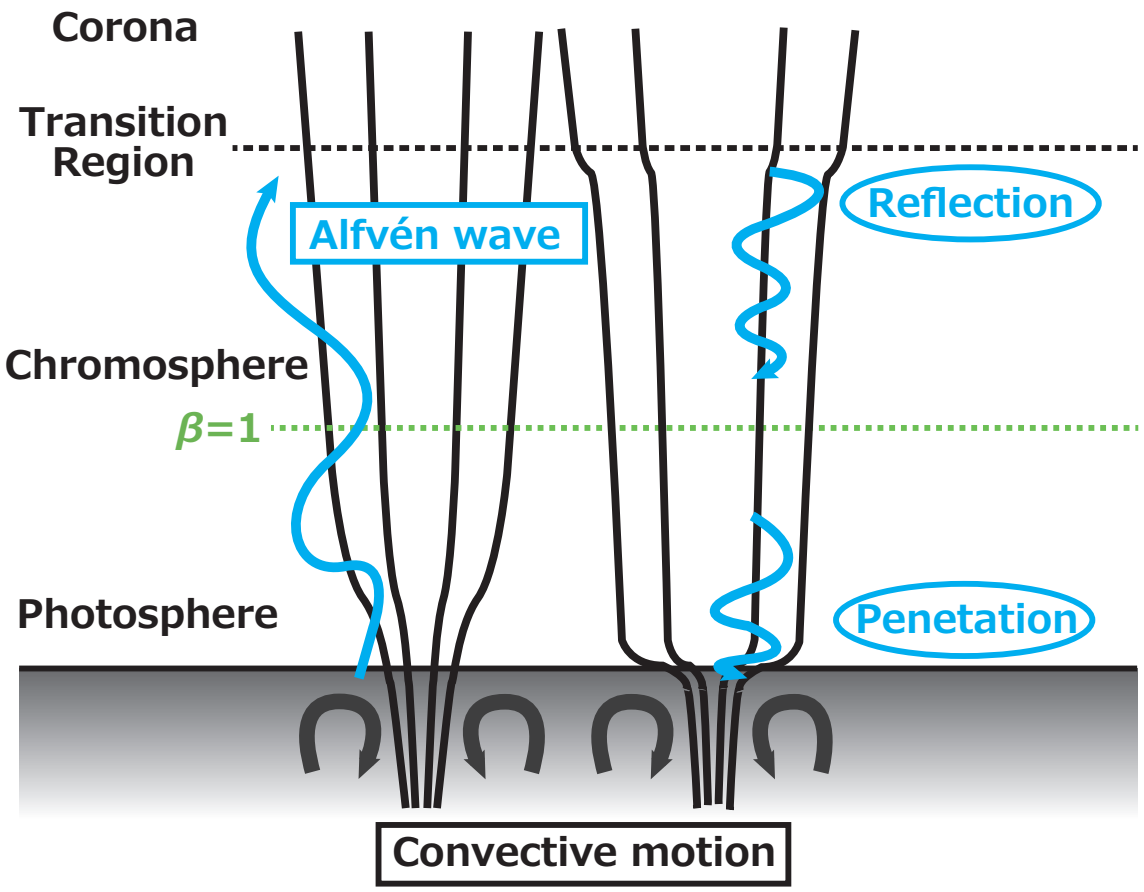

Figure 6.1: Schematic drawing of the propagation of Alfvén waves in the chromosphere along open magnetic flux tubes.

effects, the result might be changed in non-LTE condition or non-equilibrium ionization, which we should consider in detail.

We focused on the region inside the vertically open magnetic flux tube. The effect of curvature of magnetic field line has not been taken into account in our calculations. In the real solar condition, it is thought that the magnetic flux tubes are more expanding with height, and the magnetic field lines have larger curvature. We should consider such topological effects to the propagation of waves.

The formation mechanism of solar spicules is another problem and might be also future work. Under the appropriate boundary conditions at the bottom and top of the chromosphere, we investigate the formation of solar spicules in numerical simulations by setting continuous wave generator, and confirm that the properties of propagating waves along the spicules are consistent with the observational features.

Acknowledgements

I am deeply grateful to Associate Professor Takaaki Yokoyama, my supervisor, for lots of comments and suggestions throughout the course of my study. I would like to thank to all members in his laboratory, both present and graduated people, Kitagawa, N., Toriumi, S., Hotta, H., Matsui, Y., Iijima, H., Kaneko, T., Wang, S., Nasuda, T., and Shoda, M.. They gave me various useful advices and helps in my two years of study.

I would like to thank to Dr. Suzuki, T. (Nagoya Univ.), for helpful discussion and giving me prospects of the study. I also thank to Dr. Shimizu, T. (ISAS/JAXA), who organized the seminar at ISAS/JAXA. I want to express my gratitude to all members of the Space and Planetary Science Group (Univ. of Tokyo) and the Solar Terrestrial Physics Group (ISAS/JAXA). Many thanks to members in this department who encouraged me. Finally, I would like to thank to my family, for their support.

References

Athay, R. G., ed. 1976, Astrophysics and Space Science Library, Vol. 53, The solar chromosphere and corona: Quiet sun

Biermann, L. 1948, ZA, 25, 161

Braginskii, S. I. 1965, Reviews of Plasma Physics, 1, 205

De Pontieu, B., Carlsson, M., Rouppe van der Voort, L. H. M., Rutten, R. J., Hansteen, V. H., & Watanabe, H. 2012, ApJL, 752, L12

De Pontieu, B., & Haerendel, G. 1998, A&Ap, 338, 729

De Pontieu, B., Martens, P. C. H., & Hudson, H. S. 2001, ApJ, 558, 859

De Pontieu, B., et al. 2007, Science, 318, 1574

—. 2014, Science, 346, 1255732

Erdélyi, R., & James, S. P. 2004, A&Ap, 427, 1055

Fontenla, J. M., Avrett, E. H., & Loeser, R. 2002, ApJ, 572, 636

Fujimura, D., & Tsuneta, S. 2009, ApJ, 702, 1443

Gabriel, A. H. 1976, Royal Society of London Philosophical Transactions Series A, 281, 339

Gary, G. A. 2001, Sol. Phys., 203, 71

Goodman, M. L. 2011, ApJ, 735, 45

Goodman, M. L., & Kazeminezhad, F. 2010, Mem. Soc. Astron. Ital., 81, 631

Haerendel, G. 1992, Nature, 360, 241

Hahn, M., & Savin, D. W. 2014, ApJ, 795, 111

Hollweg, J. V. 1978, Sol. Phys., 56, 305

—. 1982, ApJ, 257, 345

Hollweg, J. V., Jackson, S., & Galloway, D. 1982, Sol. Phys., 75, 35

Ichimoto, K., et al. 2008, Sol. Phys., 249, 233

James, S. P., Erdélyi, R., & De Pontieu, B. 2003, A&Ap, 406, 715

Kazeminezhad, F., & Goodman, M. L. 2006, ApJS, 166, 613

Khodachenko, M. L., Rucker, H. O., Oliver, R., Arber, T. D., & Hanslmeier, A. 2006, Advances in Space Research, 37, 447

Khomenko, E., & Collados, M. 2012, ApJ, 747, 87

Kosugi, T., et al. 2007, Sol. Phys., 243, 3

Kudoh, T., & Shibata, K. 1999, ApJ, 514, 493

Lapidus, A. 1967, Journal of Computational Physics, 2, 154

Leake, J. E., Arber, T. D., & Khodachenko, M. L. 2005, A&Ap, 442, 1091

Lighthill, M. J. 1952, Royal Society of London Proceedings Series A, 211, 564

—. 1954, Royal Society of London Proceedings Series A, 222, 1

Lynch, D. K., Beckers, J. M., & Dunn, R. B. 1973, Sol. Phys., 30, 63

Matsumoto, T., & Shibata, K. 2010, ApJ, 710, 1857

Mein, N., & Mein, P. 1976, Sol. Phys., 49, 231

Mein, N., & Schmieder, B. 1981, A&Ap, 97, 310

Nishikawa, T. 1988, PASJ, 40, 613

Okamoto, T. J., & De Pontieu, B. 2011, ApJL, 736, L24

Osterbrock, D. E. 1961, ApJ, 134, 347

Parker, E. N. 1972, ApJ, 174, 499

Proudman, I. 1952, Royal Society of London Proceedings Series A, 214, 119

Rubin, E. L., & Burstein, S. Z. 1967, Journal of Computational Physics, 2, 178

Scharmer, G. B., Dettori, P. M., Lofdahl, M. G., & Shand, M. 2003, in Society of Photo-Optical Instrumentation Engineers (SPIE) Conference Series, Vol. 4853, Innovative Telescopes and Instrumentation for Solar Astrophysics, ed. S. L. Keil & S. V. Avakyan, 370–380

Schmieder, B. 1976, Sol. Phys., 47, 435

Schwarzschild, M. 1948, ApJ, 107, 1

Shimizu, T. 1995, PASJ, 47, 251

Shimizu, T., et al. 2008, Sol. Phys., 249, 221

Stein, R. F. 1968, ApJ, 154, 297

Suematsu, Y., et al. 2008, Sol. Phys., 249, 197

Suzuki, T. K., & Inutsuka, S.-i. 2005, ApJL, 632, L49

Suzuki, T. K., & Inutsuka, S.-I. 2006, Journal of Geophysical Research (Space Physics), 111, 6101

Tsuneta, S., et al. 2008, Sol. Phys., 249, 167

Unno, W., & Kato, S. 1962, PASJ, 14, 417

Vernazza, J. E., Avrett, E. H., & Loeser, R. 1981, ApJS, 45, 635

Wentzel, D. G. 1977, Sol. Phys., 52, 163

Withbroe, G. L., & Noyes, R. W. 1977, Ann. Rev. A&Ap, 15, 363

Zaqarashvili, T. V., & Erdélyi, R. 2009, Space Sci. Rev., 149, 355